RICE UNIVERSITY

PARTIAL RING CURRENTS
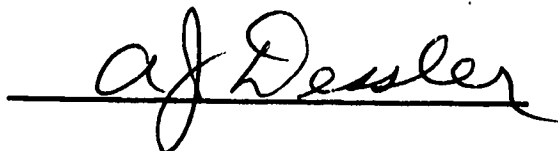
AND SOME OF THEIR GEOPHYSICAL EFFECTS

by

Warren David Cummings

A THESIS SUBMITTED
IN PARTIAL FULFILLMENT OF THE
REQUIREMENTS FOR THE DEGREE OF

DOCTOR OF PHILOSOPHY

Thesis Director's signature:

Houston, Texas

May, 1966

TABLE OF CONTENTS

INTRODUCTION

A. The Phenomenon of a Geomagnetic Storm

The fluctuations of the geomagnetic elements H, V,
and D about their quiet day values is called a geomagnetic
storm. (H is the horizontal component of the earth's
field, V is the vertical component, and D is the declina-
tion of H from true north.) Sometimes the storm can be
associated with an eruption of a solar flare that preceded
the geomagnetic phenomenon by 1 or 2 days. The storm may
last 2 or 3 days, and during this time the geomagnetic
elements may deviate from their quiet day values by as
much as $\sim$ 1%. The high-latitude fluctuations are most
erratic and exhibit large local-time variations, while the
low-latitude variations are smoother and more likely to
exhibit universal-time characteristics that are reproducible
from storm to storm.

The details of the average characteristic of
geomagnetic storms are described in <u>Chapman</u> and <u>Bartels</u>
(1940). The morphology of the low-latitude fluctuations
in H may be summarized as follows:

(a) Most storms are characterized by a <u>sudden
commencement</u> in which H increases by typically 20-30 γ,
with a rise time of 1-6 minutes. (1 γ = 10^{-5} gauss = 10^{-9}
webers/m^2 -- the earth's field at the equator is
approximately 0.3 gauss.)

(b) H remains above its pre-storm value throughout the initial phase. The initial phase lasts some two to eight hours, after which H falls below its pre-storm value.

(c) The average value of H continues to decrease during the second or main phase. Average decreases of 50 to 100 γ are typical and the main phase usually lasts from 12 to 24 hours.

(d) The recovery phase follows and may last 1 or 2 days. The recovery phase is sometimes free of geo-magnetic activity except for the steady return of H to its pre-storm value.

In addition to the above storm phases, which are seen in more or less the same form at low-latitude stations of all longitudes, one finds that the amplitude of the variations in H also depends on local-time. In particular, at low-latitude stations main phase decreases observed during the afternoon hours tend to be larger than main phase decreases observed during the morning hours. The local-time dependent part of the storm variation is called the disturbance-daily variation. An example of the phases of a storm as well as the local-time effect is shown in Figure 1.

The above morphological description of low-latitude magnetic storms is an inadequate description of the high-latitude storm. Large (typically 500 γ) and rapid fluctuations together with a pronounced local-time dependence overshadow the world-wide progression of the storm through its phases. At high latitudes there also occur large rapid fluctuations in V and D.

B. The Present Theoretical Explanation of Geomagnetic
    Storms

    Geomagnetic storm theory has been evolving for more
than one hundred years. Chapman and Bartels (1940) dis-
cuss the contributions of the early workers in the field
to ~ 1940. With the advent of space probes in the late
1950's and early 1960's the nature of the interplanetary
environment was precisely determined and several important
advances in storm theory were made. A good review of the
present theory of geomagnetic storms has been given by
Parker (1962). In the brief review that follows, emphasis
will be placed on that part of the storm theory with which
this thesis is concerned, namely the theory of the main
and recovery phases.

    .The present theory of the initial phase is based on
the idea first examined by Chapman and Ferraro (1931,
1932), that the geomagnetic storm is the result of "solar
corpuscular radiation" incident on the geomagnetic field.
The "solar corpuscular radiation", now called "solar
wind" after the work of Parker (1958, 1960) has been ob-
served with detectors aboard space vehicles (Gringauz
et al., 1960; Bridge et al., 1961).

    Since the highly ionized solar wind behaves like a
perfectly conducting fluid, the geomagnetic field is
frozen out of the stream by currents induced on its sur-
face. The geomagnetic field is thus compressed into an
elongated cavity, the boundaries of the cavity being

determined by a balance between the solar wind pressure and the geomagnetic field pressure.

The initial phase is understood to be the result of an enhanced solar wind pressure following the eruption of a solar flare. The enhanced solar wind pressure causes a compression of the geomagnetic cavity, and therefore a world-wide increase in H as measured at low latitudes.

The idea that charge particle motion in the geomagnetic field might be the cause of a storm phenomena is apparently due to Birkeland (1908, 1913). Alfven (1955) introduced the idea that currents could arise from the drift of charged particles in an inhomogeneous magnetic field, and Singer (1957) proposed that the main phase decrease could be explained in terms of the currents produced by particles trapped in the magnetosphere and drifting in the way Alfven proposed. From this point of view the main phase decrease is understood as the net magnetic effect of three currents:

1) the drift current resulting from the gradient in the geomagnetic field,

2) the drift current resulting from the curvature in the geomagnetic field,

and 3) a magnetization current determined by the distribution of the hot plasma in the magnetosphere.

It is assumed that the hot plasma responsible for the main phase decrease forms a symmetrical ring about the earth. When this is the case, each of the above three

currents flows in a ring about the earth; hence the name
"ring current" theory of the main phase.

The origin of the particles responsible for the
main phase ring current is unknown. Presumably a signi-
ficant particle pressure builds up inside the magnetosphere
during the early main phase. The particle pressure within
the magnetosphere inflates the geomagnetic field and thus
causes a decrease in H as observed at low latitudes. From
this point of view, the main phase decrease is a result
of stresses imposed on the geomagnetic field by a hot
plasma temporarily trapped within the magnetosphere (Dessler
and Parker, 1959). This hydromagnetic description of the
main phase decrease is equivalent to the drift current
explanation.

Smith (1963) has reviewed the experimental evidence
for the ring-current plasma. At the time of Smith's
article the evidence was inconclusive; recent satellite
experiments (Cahill, 1966 ;   McIlwain, 1966), however,
have apparently made unambiguous measurements of the ring
current's magnetic effects. The low energy particles that
make up the ring current belt have not yet been directly
detected.

The theory of the recovery phase is concerned with
the removal of the ring-current-particle strain on the
geomagnetic field. Parker (1962) has given a critical
review of the relaxation processes currently under discussion:

　　　　1)　scattering of the ring current particles
　　　　　　into their pitch angle loss cone by
　　　　　　hydromagnetic waves,

or 2) by coulomb scattering,

and 3) energy loss of the ring current belt by
means of a charge exchange between protons
and ambient neutral hydrogen.

The effectiveness of each of these relaxation processes depends in large part on basic ring-current parameters:

1) particle type,

2) particle energy distribution,

3) particle pitch angle distribution,

and 4) position in the magnetosphere.

Unfortunately, little is known about these basic parameters. However, the available indirect experimental observations, combined with a number of theoretical arguments, indicate the following range of values for the above parameters:

1) protons,

2) $1 < E_p < 100$ kev,

3) unknown ,

and 4) $\sim 2 < R_{RC} < \sim 6$, where R_{RC} is the geocentric
distance to the ring current belt in units
of R_E (earth radii).

With these parameters for the ring current belt, the most probable relaxation mechanism is the charge exchange process. Fite et al. (1960) have measured the total cross section for charge exchange, Q, and found that the product of Q and v, the incident proton velocity, is approximately

constant for the energy range $0.4 < E_p < 40$ kev. Liemohn
(1961) combined the cross-section measurements of Fite
et al., (1960) with a model of the terrestrial atmospheric
hydrogen distribution (Johnson and Fish, 1960) to derive
a lifetime against charge exchange:

$$\tau = (n_H Q v)^{-1}$$

At $R \approx 4R_E$, the value of τ is ~ 1 day for protons,
independent of energy in the range $1 < E_p < 100$ kev.

Chapman (1935) proposed an atmospheric current system
that could give rise to the disturbance-daily variation
part of the magnetic storm. This current system is con-
centrated in the polar regions, particularly in the auroral
zone (Figure 2). The current system is supposed to remain
fixed with respect to the earth-sun line, so that a given
station experiences a daily variation as it rotates beneath.

Fejer (1961) and Axford and Hines (1961) have
developed physical models for the Chapman current system.
However, a study by Akasofu and Chapman (1964) suggests
that the low-latitude disturbance-daily variation is not
due to the equatorward extensions of polar ionospheric
currents. Recent high-latitude magnetic observations also
are in disagreement with the original Chapman current
system (Akasofu et al., 1965). In short, the low-latitude
disturbance-daily variation is unexplained.

C. Object of this Thesis

The uniform ring current model has been fairly
successful in providing a first order explanation for the
average characteristics of the main and recovery phases
of a geomagnetic storm. However, there are many phenomena
associated with geomagnetic storms that are apparently
not related to this first-order model, e.g.,

    1)   ionospheric heating (Jacchia, 1961a,b,
         1963),

    2)   redistribution of low energy magnetospheric
         plasma (Carpenter, 1963, 1966),

    3)   redistribution of high energy magneto-
         spheric particles (Rothwell and McIlwain,
         1960; Pizzella, McIlwain, and Van Allen,
         1962 ; McIlwain, 1966).

    4)   disturbance-daily variation (Akasofu and
         Chapman, 1964),

and 5)   auroral phenomena.

There have in the past been discussions of variations
on the uniform ring current model aimed at explaining in
more detail a particular facet of the geomagnetic storm
or of some related phenomenon, e.g.,

    1)   the recovery phase (Akasofu, Chapman,
         and Venkatesan, 1963),

2) the disturbance-daily variation (Shaw,
1959; Fejer, 1961, 1963; Vestine, 1960;
Kern, 1961; Akasofu and Chapman, 1964),

and 3) auroral phenomena (Kern, 1962; Swift,
1963, 1964; Akasofu, 1964).

In this thesis a non-uniform ring current model is
explored. The various effects of small scale energy
density fluctuations in the ring current belt are discussed.
In particular, we examine storm related atmospheric heat-
ing as a consequence of a non-uniform ring current belt.

We also discuss the magnetic effects of a large
scale asymmetry in the ring current belt. We show that a
simple asymmetric ring current model can explain most of
the low-latitude disturbance-daily variation.

FIGURE 1:   A sample magnetic storm. As observed
             at San Juan, the storm shows clearly
             the initial, main, and recovery phases.
             The main phase decrease at San Juan is
             more than 200 γ , while at Honolulu, it
             is only about 100 γ . This descrepancy
             is attributed to the disturbance-daily
             variation. Note that the main phase
             at San Juan is centered about the after-
             noon hours, which are the morning hours
             for Honolulu.

FIGURE 2:   The idealized Chapman current system
             (from Chapman and Bartels, p. 302).
             Most of the current is concentrated in
             the polar regions where the disturbance
             daily variation is the dominant effect
             during a magnetic storm. The low
             latitude variation is caused by the
             equatorward extensions of the polar
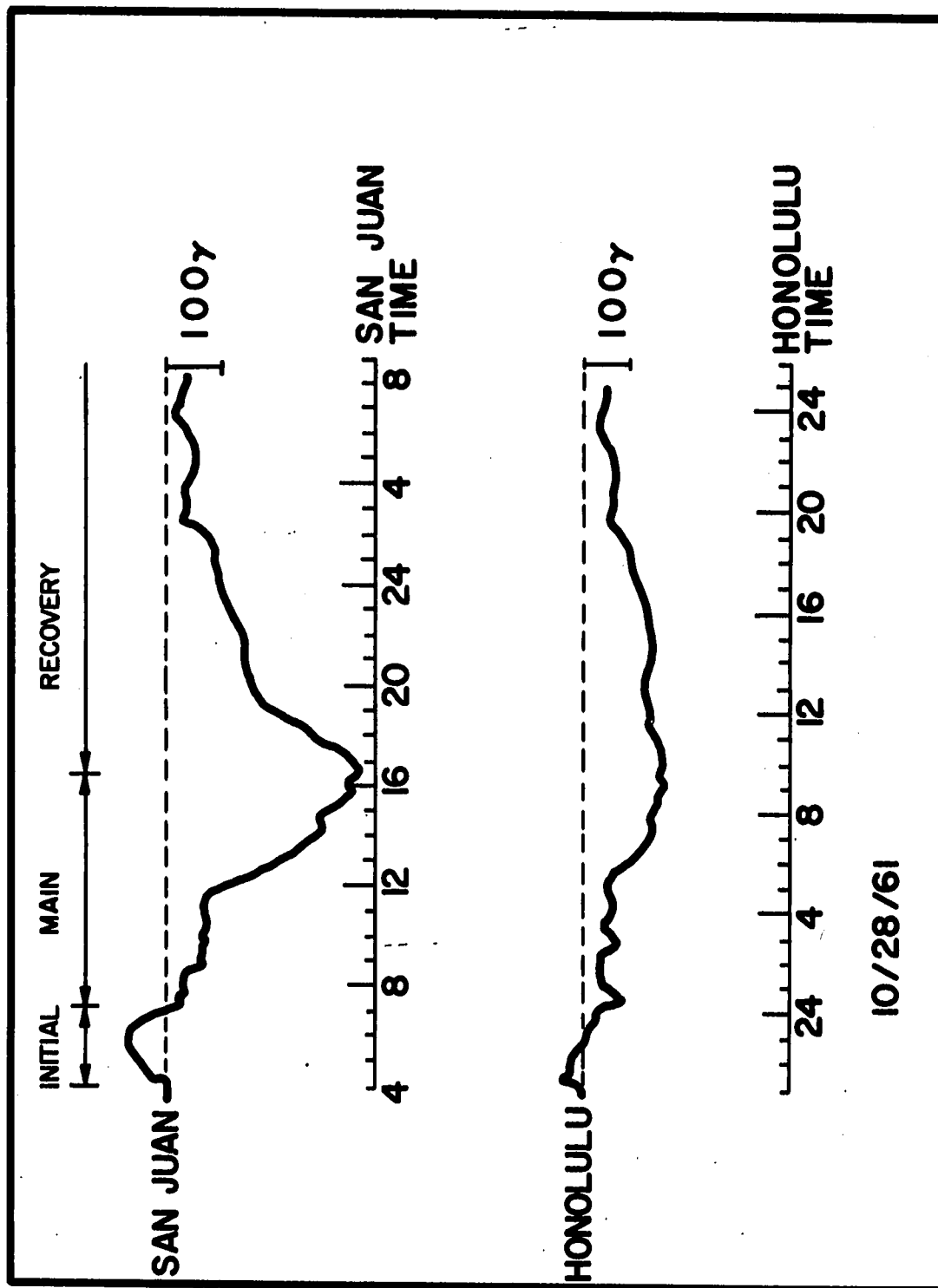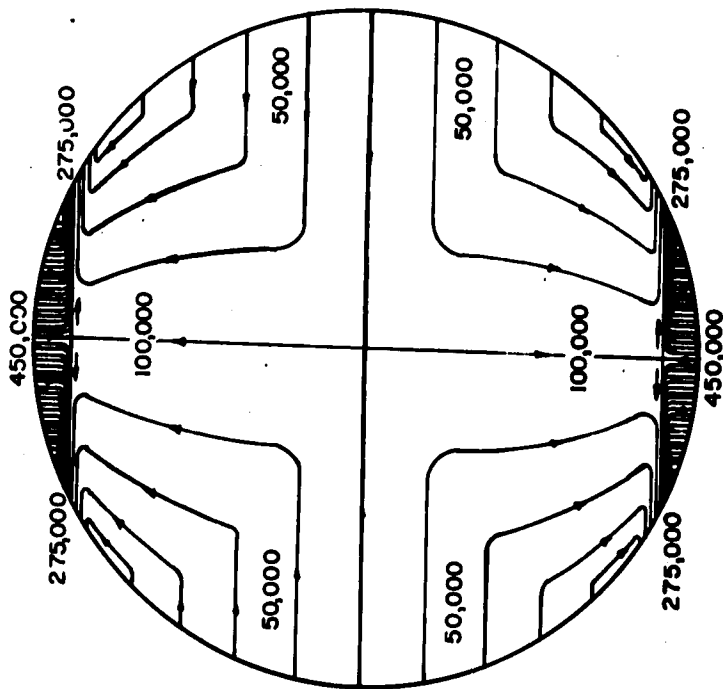   currents, according to this explanation.
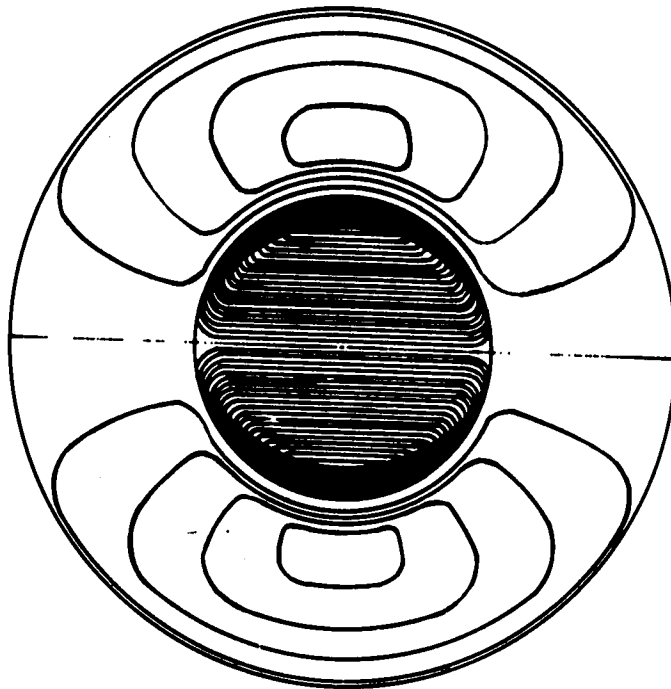
FIGURE 1

FIG.B. VIEW FROM ABOVE THE NORTH POLE

FIG.A VIEW FROM THE SUN

P 54 259

FIGURE 2

NON-UNIFORM RING CURRENTS

A. A Survey of the Problem

In this section we briefly survey the consequences of an energy density enhancement in the ring current belt. Each of the aspects of the problem that are introduced in this section will be developed in more detail in subsequent sections.

In studying uniform ring currents from the single particle orbit theory approach, one is concerned with three current densities:

$$\bar{j}_G = u_\perp \frac{\bar{B} \times \overline{\nabla B}}{B^3} \quad \text{(m.k.s. units) Gradient B current,} \quad 1)$$

$$\bar{j}_R = 2u_\parallel \frac{\bar{R}_c \times \bar{B}}{R_c^2 B^2} \quad \text{Curvature current,} \quad 2)$$

$$\bar{j}_M = \text{curl } \bar{M} = \text{curl} \left(-\frac{u_\perp \bar{B}}{B^2} \right) \quad \text{Magnetization current,} \quad 3)$$

where :

$u_\perp$ = the particle kinetic energy density of motion perpendicular to the magnetic field,

$u_{||}$ = the particle kinetic energy density of motion parallel to the magnetic field,

$\bar{B}$ = the magnetic field vector,

$\bar{R}_c$ = the radius of curvature of the field lines,

and

$\bar{M}$ = the magnetization of the ring current plasma.

The current densities $\bar{j}_G$ and $\bar{j}_R$ arise from drift motion of the center of rotation, i.e., the guiding center, of the ring current particles. A gradient in the magnetic field causes a drift of the guiding center with velocity:

$$\bar{v}_G = w_\perp \frac{\bar{B} \times \overline{\nabla B}}{eB^3} \qquad \text{Gradient drift velocity} \quad 4)$$

and a curvature in the B lines causes a drift of the guiding center with the velocity:

$$\bar{v}_R = 2w_{||} \frac{\bar{R}_c \times \bar{B}}{eR_c^2 B^2} \qquad \text{Curvature drift velocity} \quad 5)$$

where:

$w_\perp$ = the particle kinetic energy due to
motion perpendicular to $\bar{B}$,

$w_{||}$ = the particle kinetic energy due to
motion parallel to $\bar{B}$,

and

e = the charge of the ring current particle.

The circular motion of a charged particle in the
magnetic field $\bar{B}$ produces a magnetic moment given by:

$$\bar{I}_1 = - \frac{w_\perp}{B^2} \bar{B} \quad .$$

The magnetization of the plasma is just the magnetic
moment per unit volume, or :

$$\bar{M} = n\bar{I}_1 = - \frac{u_\perp \bar{B}}{B^2} \quad ,$$

where :

n = number density of the ring current particles.

If the magnetic field is assumed to have zero curl, i.e., if the perturbation of the geomagnetic field by the ring current plasma is assumed negligible, then we have :

$$\text{div}(\bar{j}_G) = \frac{(\bar{B} \times \overline{\nabla B}) \cdot \overline{\nabla u}_{\perp}}{B^3}$$

$$\text{div}(\bar{j}_R) = \frac{2(\bar{R}_C \times \bar{B}) \cdot \overline{\nabla u}_{\parallel}}{R_C^2 B^2}$$

$$\text{div}(\bar{j}_M) \equiv 0 \quad .$$

A uniform ring current belt, in the curl-free field approximation, may be defined as one in which :

$$(\bar{B} \times \overline{\nabla B}) \cdot \overline{\nabla u}_{\perp} \equiv 0$$

and

$$(\bar{R}_C \times \bar{B}) \cdot \overline{\nabla u}_{\parallel} \equiv 0 \quad .$$

There is never any build up of charge within such a plasma, since :

$$\frac{\partial \rho}{\partial t} = -\text{div}(\bar{j}) \equiv 0$$

A non-uniform ring current belt may be defined as one in which:

$$(\bar{B} \times \overline{\nabla B}) \cdot \overline{\nabla u}_{\perp} \neq 0$$

and

$$(\bar{R}_c \times \bar{B}) \cdot \overline{\nabla u}_{\parallel} \neq 0 \ .$$

Since $\text{div}(\bar{j}_G)$ and $\text{div}(\bar{j}_R)$ are no longer necessarily zero, the charge density at any point within the belt may change with time. It is therefore possible to have time dependent electric fields in a non-uniform ring current belt.

The presence of ring current electric fields in a magnetosphere pervaded by a low temperature background plasma means that the behavior of the ring current belt will be influenced by the ionosphere. Because of the background plasma, the geomagnetic field lines are almost perfect conductors parallel to B. The field lines may be regarded as equipotential lines, and therefore a potential difference developed between field lines in the magnetosphere will also appear in the ionosphere. The subsequent development of the magnetospheric potential difference, and hence of its effect on the ring current belt, will depend to some extent on the response of the ionosphere.

The presence of electric fields in the ring current belt and consequently in the ionosphere, makes it necessary to consider two more current densities:

$$\bar{j}_P = \frac{\rho_m \dot{\bar{E}}}{B^2} \quad (\bar{E} \perp \bar{B}) \qquad \text{Polarization current} \qquad 6)$$

and

$$\bar{j}_I = \sigma_1 \bar{E} \quad (\bar{E} \perp \bar{B}) \qquad \text{Pederson current} \qquad 7)$$

where :

ρ_m = the <u>total</u> plasma mass density,

$\bar{E}$ = the electric field vector,

and

σ_1 = the Pederson, or reduced, conductivity.

The polarization current results from the pulling apart of positive and negative charges by a changing electric field. The quantity $\frac{\rho_m}{B^2} \equiv \epsilon$ may be regarded as the low frequency magnetic plasma permittivity. It is related to the hydromagnetic wave velocity by the expression:

$$v_{hm} = \frac{B^2}{\sqrt{\mu_o \rho_m}} = \frac{1}{\sqrt{\mu_o \epsilon}} \quad .$$

The Pederson current is just an Ohm's law current. The Pederson conductivity takes into account the effect of both particle collisions and a transverse magnetic field in retarding the current. For low frequency electric

fields, the Pederson conductivity is a sharply peaked function of altitude, having a maximum in the ionosphere (Figure 3).

In Figure 4 we have summarized the consequences of an energy density enhancement in the ring current belt. The effect of the drift currents, $\bar{j}_G$ and $\bar{j}_R$, is to build up charge at the boundaries of the enhancement, while the effect of the currents $\bar{j}_P$ and $\bar{j}_I$ is to diminish this charge. All of the currents flow perpendicularly to the magnetic field.

In addition to causing the polarization and Pederson currents, a ring current belt electric field gives rise to the electric drift velocity:

$$\bar{v}_E = \frac{\bar{E} \times \bar{B}}{B^2} \qquad \text{Electric drift velocity.} \qquad 8)$$

This drift of the plasma does not give rise to a current. The drift is not confined to the particles that create the electric field; all particles, independent of energy, assume the electric drift velocity.

The electric field associated with an energy density enhancement is eastward as viewed from the earth. The electric drift velocity of the enhancement is therefore outward as viewed from the earth, i.e., energy density enhancements tend to be ejected from the ring current belt. The velocity of ejection will depend, among other things,

on the strength of the electric field, and hence on the magnitude of the ionospheric conductivity. For example, if the ionospheric Pederson conductivity is infinite the electric field associated with an enhancement will be "shorted out" and the ejection velocity will be zero.

The ionospheric conductivity need not be infinite to prevent the loss of an energy density enhancement from the ring current belt. The non-uniform ring current belt is stabilized if the conductivity is high enough so that typical electric drift velocities are less than the gradient and curvature drift velocities that characterize the belt.

If the ionospheric conductivity is not high enough to stabilize the ring current belt some of the particle energy lost from the belt may appear in the ionosphere. The ring current particle energy appears in the ionosphere as Joule heating from the stabilizing currents.

FIGURE 3:   The Pederson conductivity as a function
             of altitude for four points in the
             sunspot and day-night cycles. These
             curves are from <u>Hanson</u> (1965).

FIGURE 4:   A summary of the consequences of an
             energy density enhancement in the ring
             current belt. The enhancement is repre-
             sented by the shaded region. The curva-
             ture and gradient drift currents tend to
             build up charge on the boundaries of the
             enhancement, and the polarization and
             Pederson currents tend to diminish this
             charge build up. The tube of flux
             associated with the enhancement assumes
             the electric drift velocity given in
             magnitude by $v_E = \dfrac{E}{B}$.
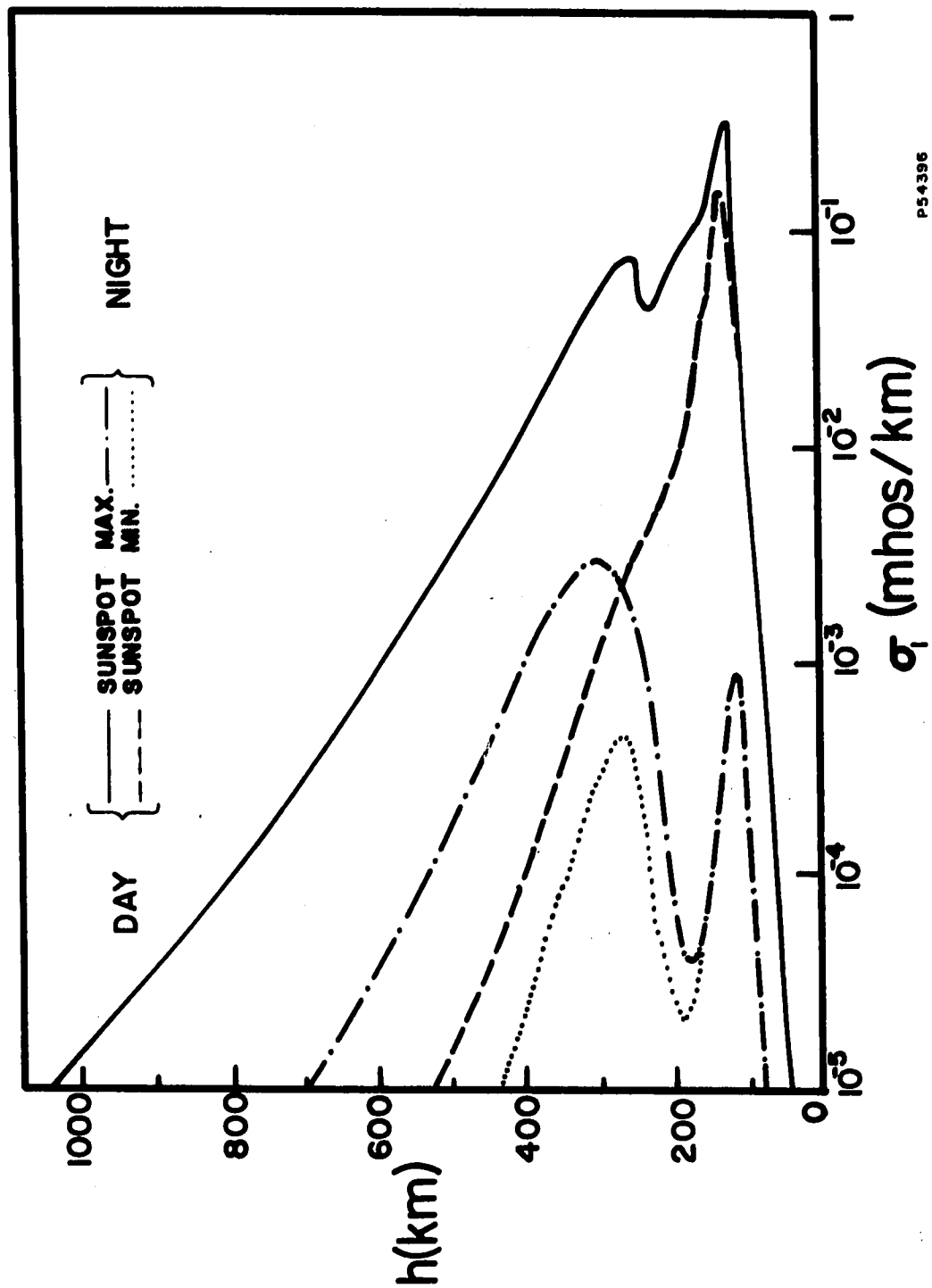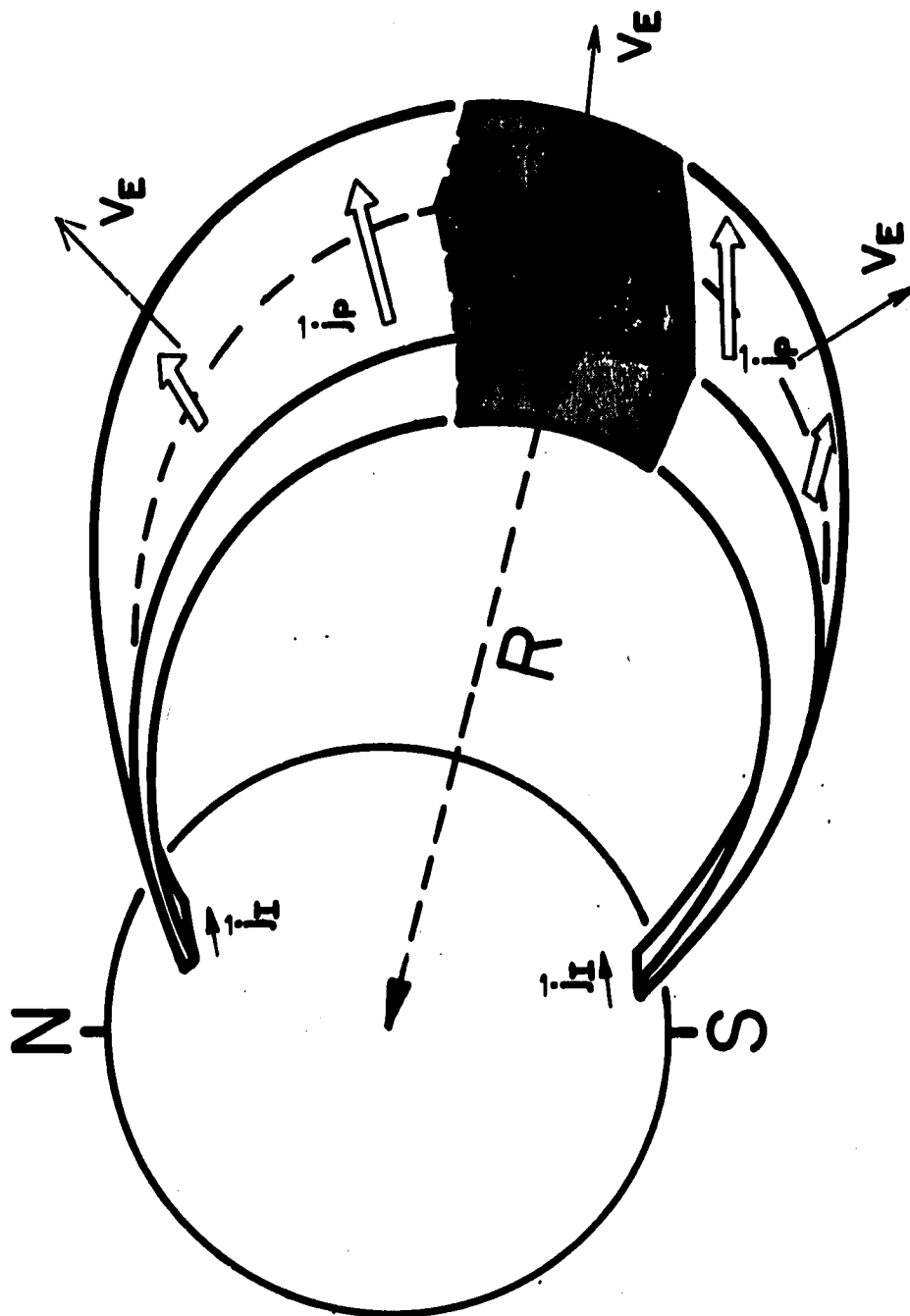
FIGURE 3

FIGURE 4

P54093B

B. The Model Used for Calculations

In order to proceed beyond a qualitative discussion, it is necessary to make calculations based on some model of the magnetosphere and ring current belt. In this section we list the assumptions of the model used in this thesis and briefly discuss some of the consequences of these assumptions:

We assume:

1) the ring current belt energy content is sufficiently low to allow a curl-free (dipole) magnetic field approximation,

2) the background low temperature plasma is always able to maintain a given magnetic field line as an equipotential,

3) the magnetic-moment and bounce actions (I_1 and I_2) of the ring current particles are invariant.

and 4) energy density enhancements in the ring current belt are in the shape of tubes of flux; the ring current particles have pitch angle and energy distributions such that:

$$\int_0^\infty w n_{eq}(w, \alpha_{eq}) \, dw = \frac{u_{eq} \sin^\delta \alpha_{eq}}{2\pi \int_0^{\pi/2} \sin^{\delta+1} \alpha_{eq} \, d\alpha_{eq}} \quad ,$$

where:

w = particle energy,

α_{eq} = particle pitch angle in the equatorial plane,

$n_{eq}(w,\alpha_{eq})$ = equatorial number density per unit solid angle and per unit energy,

and

δ = a parameter that characterizes the pitch angle distribution of the ring current particles.

Since we are making a dipole approximation for the magnetic field, we can facilitate calculations by choosing a special dipole coordinate system. In addition to the ordinary spherical polar coordinate system we will occasionally use an orthogonal dipole coordinate system having the following properties: Any point in space is determined by three numbers (P, R, φ), where P and R are related to the spherical polar coordinates r and θ by the equations:

$$r = P \sqrt{|\cos \theta|} \qquad\qquad 9)$$

and

$$r = R \sin^2 \theta \qquad\qquad 10)$$

Curves of constant P and constant R are shown in Figure 5. The curves of constant R are just the ordinary dipole lines, and in subsequent calculations they will be assumed identical with the earth's field lines. The curves of constant P are the orthogonal trajectories of the dipole lines. The coordinate φ in the dipole system is the same as φ in the spherical polar coordinate system.

The element of length along a curve of constant R is given by the expression:

$$dS_R = R \sin \theta (1 + 3 \cos^2 \theta)^{\frac{1}{2}} d\theta \; .$$

11)

The element of length along a curve of constant P is given by:

$$dS_P = - \frac{P(1 + 3 \cos^2 \theta)^{\frac{1}{2}} d\theta}{2 \sqrt{|\cos \theta|}} \; ,$$

12)

or

$$dS_P = \frac{|\sin^3 \theta| \, dR}{(1 + 3 \cos^2 \theta)^{\frac{1}{2}}} \; .$$

13)

The element of area in a plane of constant φ is given by:

$$dA_\varphi = dS_R \, dS_P = R \sin^4 \theta \, d\theta \, dR \ , \qquad 14)$$

and the element of area in a surface of constant P is given by:

$$dA_P = r \sin \theta \, d\varphi \, dS_P \ , \qquad 15)$$

or

$$dA_P = \frac{P^2}{2} (1 + 3 \cos^2 \theta)^{\frac{1}{2}} \sin \theta \, d\theta \, d\varphi \ , \qquad 16)$$

or

$$dA_P = \frac{R \sin^6 \theta \, d\varphi \, dR}{(1 + 3 \cos^2 \theta)^{\frac{1}{2}}} \ . \qquad 17)$$

The differential volume element is given by:

$$dV = r \sin \theta \, dS_R \, dS_P \, d\varphi = R^2 \sin^7 \theta \, d\theta \, dR \, d\varphi \ . \quad 18)$$

For future reference, we also note that the variation
of field strength along a line of constant R is given by:

$$B = B_{eq} \frac{(1 + 3 \cos^2 \theta)^{\frac{1}{2}}}{\sin^6 \theta} \quad , \tag{19}$$

where:

B_{eq} = the equatorial magnetic field strength
at a distance R from the center of
the earth.

The variation of the radius of curvature along a line of
force is given by:

$$R_c = \frac{R \sin \theta (1 + 3 \cos^2 \theta)^{\frac{3}{2}}}{3(1 + \cos^2 \theta)} \quad . \tag{20}$$

Since we are assuming the geomagnetic field lines
are equipotentials, the potential difference, $\Delta \psi$, between
two adjacent field lines with the same value of R is
independnet of θ . The (longitudinal) electric field
associated with such a potential difference is a simple
function of θ . We have:

$$\bar{E}(R,\theta,\varphi) \;=\; \frac{\Delta\psi(R,\theta,\varphi)\,\bar{e}_\varphi}{R\,\sin^3\theta\,\Delta\varphi}$$

$$=\; \frac{\Delta\psi(R,\theta\,',\varphi)\,\bar{e}_\varphi}{R\,\sin^3\theta\,\Delta\varphi}$$

$$=\; \frac{\sin^3\theta\,'\Delta\psi(R,\theta\,',\varphi)\,\bar{e}_\varphi}{\sin^3\theta\;R\,\sin^3\theta\,'\Delta\varphi} \;\;.$$

Hence:

$$\bar{E}(R,\theta,\varphi) \;=\; \frac{\sin^3\theta\,'}{\sin^3\theta}\;\bar{E}(R,\theta\,',\varphi) \;\;. \qquad\qquad 21)$$

The charge density along a dipole field line is also simply related to the charge density at any other point along the same line. We have:

$$\rho(R,\theta,\varphi) \;=\; \epsilon_0 \; \text{div} \; \bar{\bar{E}}(R,\theta,\varphi)$$

$$=\; \frac{\epsilon_0}{R \sin^3 \theta} \; \frac{\partial E(R,\theta,\varphi)}{\partial \varphi}$$

$$=\; \frac{\epsilon_0 \sin^3 \theta'}{R \sin^6 \theta} \; \frac{\partial E(R,\theta',\varphi)}{\partial \varphi}$$

$$=\; \frac{\epsilon_0 \sin^6 \theta'}{\sin^6 \theta} \; \frac{1}{R \sin^3 \theta'} \; \frac{\partial E(R,\theta',\varphi)}{\partial \varphi}$$

$$=\; \frac{\epsilon_0 \sin^6 \theta'}{\sin^6 \theta} \; \text{div} \; \bar{\bar{E}}(R,\theta',\varphi) \quad .$$

Hence:

$$\rho(R,\theta,\varphi) \;=\; \frac{\sin^6 \theta'}{\sin^6 \theta} \; \rho(R,\theta',\varphi) \quad . \qquad\qquad 22)$$

As we will see in subsequent sections, it will be necessary to integrate particle energy density along a tube of flux. The assumption that the pitch angle and energy distributions are separable (3), together with the assumption that I_1 and I_2 are invariant (4), simplifies these integrations. We now derive (following Longmire, p.58, 1963) expressions for $u_\parallel$ and $u_\perp$ as a function of position along a tube of flux.

Let $n^+_{eq}(w, I_1) \, dw \, dI_1$ be the equatorial number density of particles moving along the tube toward the north magnetic pole and having total energy w in dw and magnetic moment I_1 in dI_1. The particles move along the tube of force with velocity $v_\parallel$ given by:

$$v_\parallel = \sqrt{\left(\frac{2}{m}\right)(w - I_1 B)} \quad ,$$

where:

$$m = \text{particle mass.}$$

Since the cross-sectional area of the flux tube is proportional to $\frac{1}{B}$, we must have for any point along the tube that is accessible to particles with magnetic moment I_1:

$$n^+(w, I_1)\frac{v_\parallel}{B} = \text{constant} = n^+_{eq}(w, I_1)\frac{v_{\parallel eq}}{B_{eq}} \quad ,$$

or

$$n^+(w, I_1) = n_{eq}^+(w, I_1) \frac{v_{\|eq}}{v_\|} \frac{B}{B_{eq}} \quad .$$

The part of $u_\|$ that arises from particles with energy w and magnetic moment I_1 moving toward the north pole is given by:

$$u_\|^+(w, I_1) = n^+(w, I_1)(\tfrac{1}{2} mv_\|^2)$$

$$= \frac{n_{eq}^+(w, I_1) mv_{\|eq}}{2} v_\| \frac{B}{B_{eq}}$$

$$= n_{eq}^+(w, I_1) w \frac{B \sqrt{\left(1 - \frac{I_1}{w} B_{eq}\right)\left(1 - \frac{I_1}{w} B\right)}}{B_{eq}} \quad .$$

For the pitch angle distributions under consideration an equal contribution to $u_\|$ is provided by particles moving toward the south pole. We therefore have:

$$u_\| = \int_0^{\frac{w}{B}} \int_0^\infty n_{eq}(w, I_1) w \frac{B \sqrt{\left(1 - \frac{I_1}{w} B_{eq}\right)\left(1 - \frac{I_1}{w} B\right)}}{B_{eq}} \, dw \, dI_1$$

where:

$$n_{eq}(w, I_1) = n_{eq}^+(w, I_1) + n_{eq}^-(w, I_1) \quad .$$

Since:

$$I_1 = \frac{w}{B_{eq}} \sin^2 \alpha_{eq} \quad ,$$

we can define $n_{eq}(w, \alpha_{eq})$ by:

$$n_{eq}(w, \alpha_{eq}) 2\pi \sin \alpha_{eq} \, d\alpha_{eq} \equiv n_{eq}(w, I_1) \, dI_1 \quad ,$$

and write:

$$u_{\parallel} = \int_0^{\sin^{-1} \sqrt{\frac{B_{eq}}{B}}} \int_0^{\infty} \left[n_{eq}(w, \alpha_{eq}) w \frac{B}{B_{eq}} \cos \alpha_{eq} \cdot \right.$$

$$\left. \sqrt{1 - \frac{B}{B_{eq}} \sin^2 \alpha_{eq}} \, (2\pi \sin \alpha_{eq}) \right] \, dw \, d\alpha_{eq} \quad ,$$

or

$$u_{\parallel} = \frac{u_{eq}\left(\frac{B}{B_{eq}}\right)^{\frac{3}{2}}}{\left(\int_{0}^{\pi/2} \sin^{\delta+1}\alpha_{eq}\, d\alpha_{eq}\right)} \int_{0}^{\sin^{-1}\sqrt{\frac{B_{eq}}{B}}} \left[\sqrt{\sqrt{\frac{B_{eq}}{B}} - \sin^2\alpha_{eq}} \right. \cdot$$

$$\left. \sin^{\delta+1}\alpha_{eq}\cos\alpha_{eq}\right] d\alpha_{eq} \quad ,$$

or

$$u_{\parallel} = \frac{u_{eq}\left(\frac{B}{B_{eq}}\right)^{\frac{3}{2}}}{\left(\int_{0}^{\pi/2} \sin^{\delta+1}\alpha_{eq}\, d\alpha_{eq}\right)} \int_{0}^{\sqrt{\frac{B_{eq}}{B}}} \sqrt{\frac{B_{eq}}{B} - x^2}\ x^{\delta+1}\, dx \ . \quad 22)$$

We can similarly derive an expression for $u_{\perp}$. The part of $u_{\perp}$ that arises from particles with energy w and magnetic moment I_1 is given by:

$$u_{\perp}(w,I_1) = n_{eq}(w,I_1)(\tfrac{1}{2} m v_{\perp}^2)\frac{v_{\parallel eq}}{v_{\parallel}} \ \frac{B}{B_{eq}}$$

$$= n_{eq}(w,I_1)I_1 \frac{B^2}{B_{eq}} \sqrt{\frac{1 - \frac{I_1}{w}B_{eq}}{1 - \frac{I_1}{w}B}}$$

Hence:

$$
u_\perp = \int_0^{\frac{w}{B}} \int_0^\infty n_{eq}(w, I_1) I_1 \frac{B^2}{B_{eq}} \sqrt{\frac{1 - \frac{I_1}{w} B_{eq}}{1 - \frac{I_1}{w} B}} \; dw \; dI_1
$$

$$
= \int_0^{\sin^{-1}\sqrt{\frac{B_{eq}}{B}}} \int_0^\infty \left[n_{eq}(w, \alpha_{eq}) w \frac{B^2}{B_{eq}^2} \sin^2 \alpha_{eq} \right. \cdot
$$

$$
\left. \frac{\cos \alpha_{eq}(2\pi \sin \alpha_{eq})}{\sqrt{1 - \frac{B}{B_{eq}} \sin^2 \alpha_{eq}}} \right] dw \; d\alpha_{eq}
$$

$$
= \frac{u_{eq} \left(\frac{B}{B_{eq}}\right)^{\frac{3}{2}} \displaystyle\int_0^{\sin^{-1}\sqrt{\frac{B_{eq}}{B}}} \frac{\sin^{3+\delta} \alpha_{eq} \cos \alpha_{eq} \, d\alpha_{eq}}{\sqrt{\frac{B_{eq}}{B} - \sin^2 \alpha_{eq}}}}{\left(\displaystyle\int_0^{\pi/2} \sin^{\delta+1} \alpha_{eq} \, d\alpha_{eq}\right)} \quad ,
$$

or

$$u_\perp = \cfrac{u_{eq} \left(\dfrac{B}{B_{eq}}\right)^{\frac{3}{2}} \displaystyle\int_0^{\sqrt{\frac{B_{eq}}{B}}} \dfrac{x^{3+\delta}\, dx}{\sqrt{\dfrac{B_{eq}}{B} - x^2}}}{\left(\displaystyle\int_0^{\pi/2} \sin^{\delta+1} \alpha_{eq}\, d\alpha_{eq}\right)} \qquad \cdot$$

Expressions for $u_\parallel$ and $u_\perp$, for $\delta = 0, 1, 2,$ and 3, are given in Table 1.

Finally, we note that if I_1 and I_2 are conserved, the equatorial pitch angle and energy variations with R can be calculated. The relevant equations are:

$$I_1 = \frac{w \sin^2 \alpha_{eq}}{B_{eq}} \qquad\qquad 24)$$

and

$$I_2 = m \oint v \cos \alpha\, dS_R \quad , \qquad\qquad 25)$$

where the integration is over a complete north-south oscillation.

Substituting:

$$dS_R = R \sin \theta (1 + 3 \cos^2 \theta)^{\frac{1}{2}} d\theta \quad , \qquad\qquad 11)$$

$$v = \sqrt{\frac{2w}{m}} \quad ,$$

and

$$\cos \alpha = \sqrt{1 - \frac{BI_1}{w}}$$

$$= \sqrt{1 - \sin^2 \alpha_{eq} \frac{(1 + 3 \cos^2 \theta)^{\frac{1}{2}}}{\sin^6 \theta}}$$

into eq.(25) yields:

$$I_2 = \sqrt{w} \, RF(\alpha_{eq}) \quad , \qquad\qquad 26)$$

where:

$$F(\alpha_{eq}) = 4\sqrt{2m} \int_0^{\theta_m} \left\{ \left[1 - \frac{\sin^2 \alpha_{eq}(1 + 3 \cos^2 \theta)^{\frac{1}{2}}}{\sin^6 \theta} \right] \cdot \right.$$

$$\left. \left[1 + 3 \cos^2 \theta \right] \right\}^{\frac{1}{2}} \sin \theta \, d\theta \quad ,$$

and θ_m is given by:

$$1 - \frac{\sin^2 \alpha_{eq}(1 + 3\cos^2 \theta_m)^{\frac{1}{2}}}{\sin^6 \theta_m} = 0 \quad .$$

The changes in α_{eq} with R can be computed from the equation:

$$\frac{I_1}{I_2} = \frac{\sin^2 \alpha_{eq}}{B_{eq} R^2 F^2(\alpha_{eq})} \quad , \qquad 27)$$

and once α_{eq} is known, w can be computed from either of the action invariant equations.

Figures 6 and 7, taken from a paper by Nakada et al., (1965) illustrate the functional dependence of α_{eq} and w on R .

The assumptions discussed in this section are the main ones used in the thesis. Others, such as the neglect of a latitude dependence in the ionospheric conductivity, are more restricted in their influence and will be discussed individually.

FIGURE 5:   The dipole coordinate system. Curves
                 of constant R are dipole lines.
                 Curves of constant P are orthogonal
                 trajectories to the dipole lines.

FIGURE 6:   The variation of equatorial pitch angle
                 with geocentric radial distance if I_1
                 and I_2 are conserved (from Nakada
                 et al., 1965).

FIGURE 7:   The variation of particle energy with
                 geocentric radial distance. The curves
                 are normalized to particle energy at
                 $R = 7R_E$. Pitch angles characterizing
                 each curve refers to the equatorial
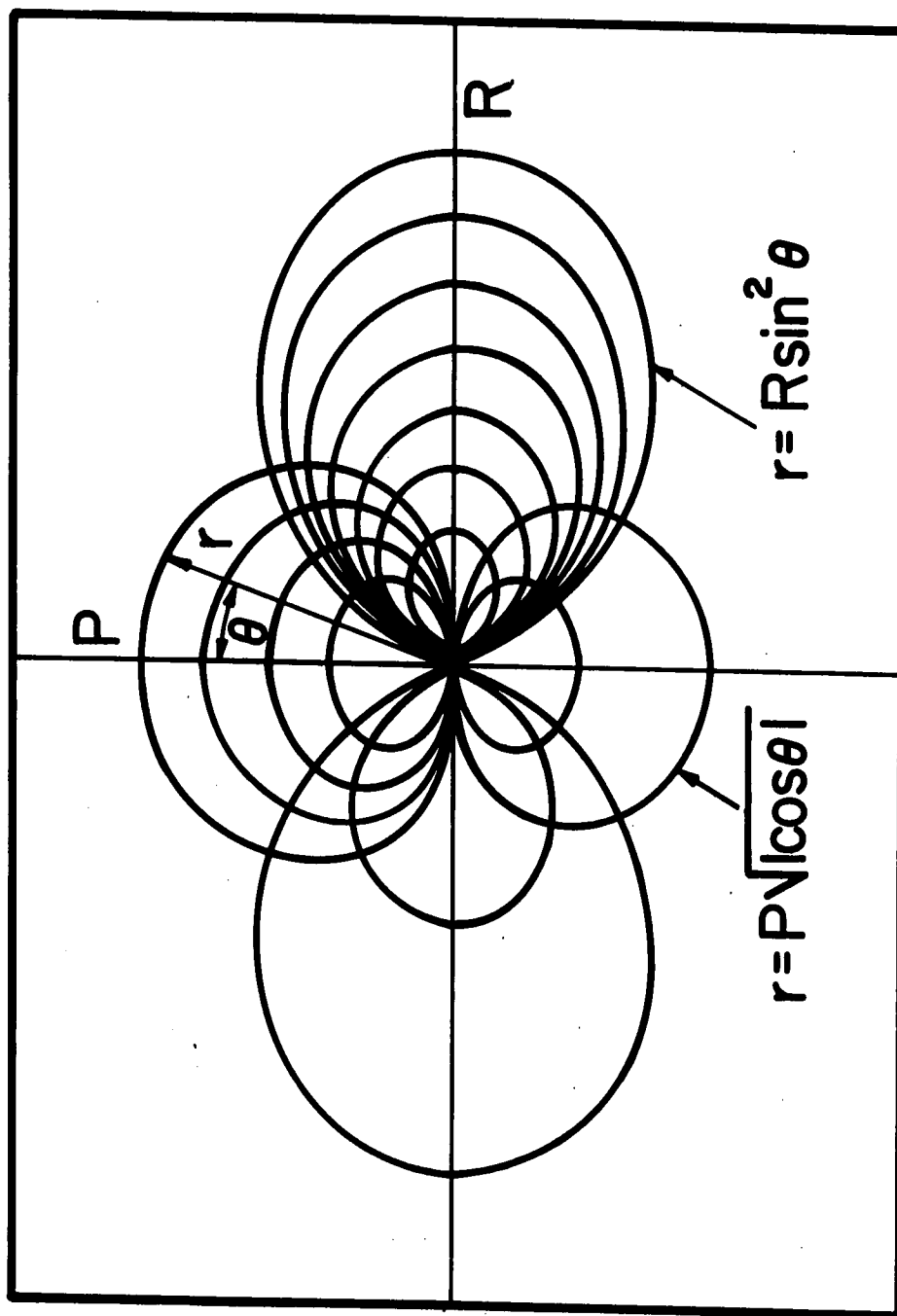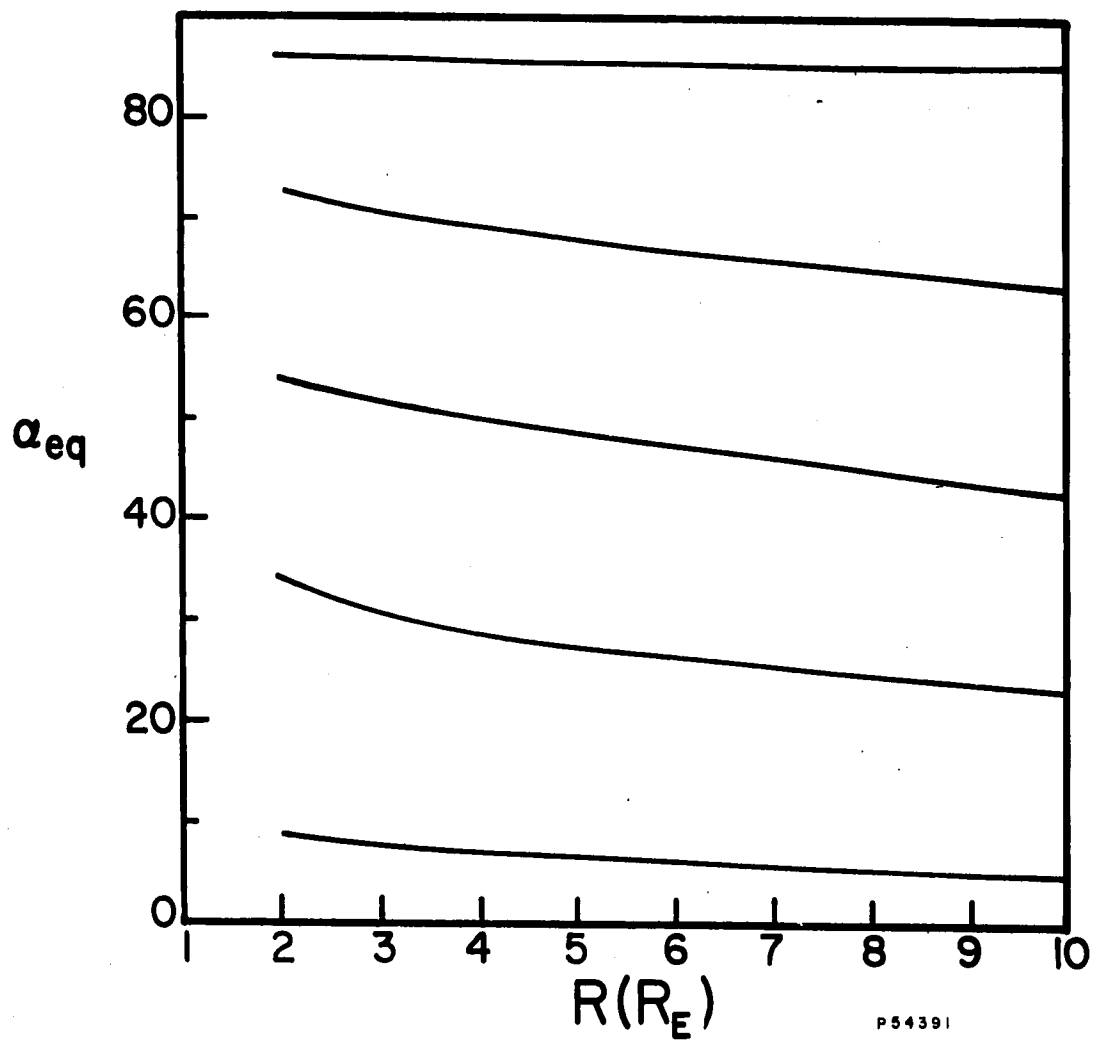   pitch angle at $R = 7R_E$ (from Nakada
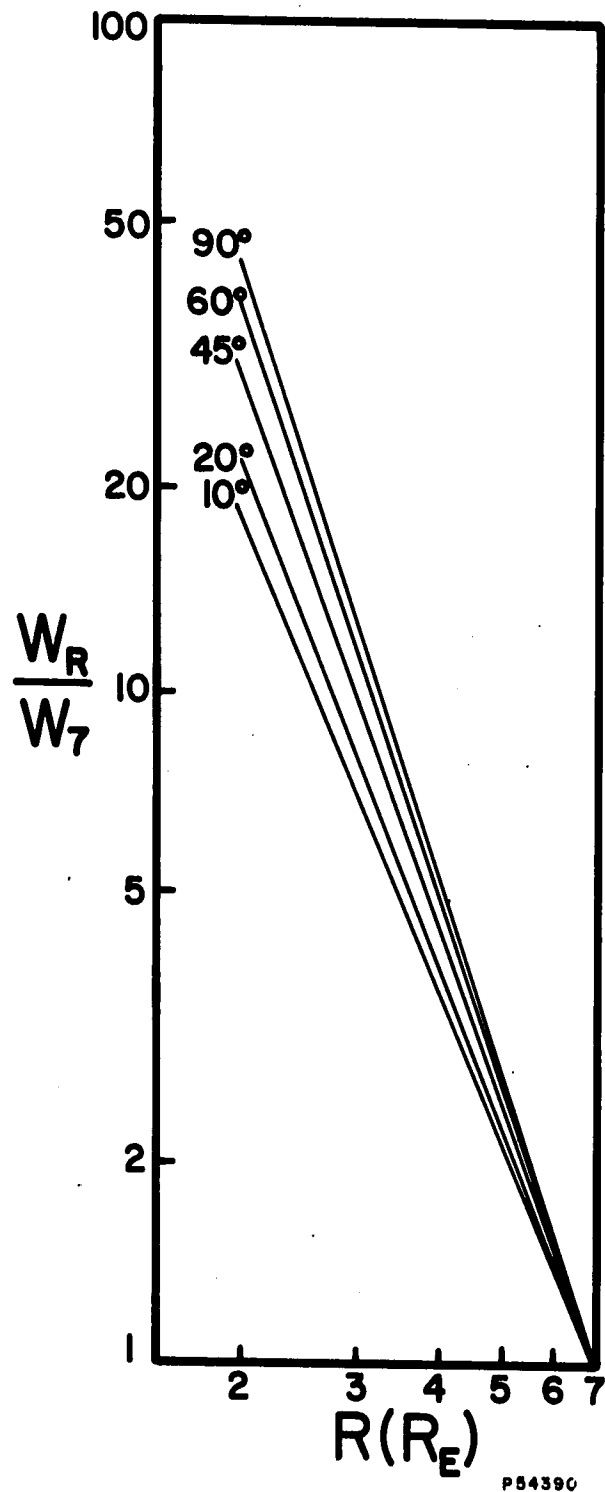   et al., 1965).

$$r = R\sin^2\theta$$

$$r = P\sqrt{|\cos\theta|}$$

FIGURE 5

P54394

FIGURE 6

P54390

FIGURE 7

TABLE 1. The perpendicular and parallel components of the energy density for four values of the pitch angle parameter.

δ	$u_\perp$	$u_{\parallel}$
0	$\frac{2}{3} u_{eq}$	$\frac{1}{4} u_{eq}$
1	$\frac{3}{4} u_{eq} \left(\frac{B_{eq}}{B} \right)^{\frac{1}{2}}$	$\frac{1}{4} u_{eq} \left(\frac{B_{eq}}{B} \right)^{\frac{1}{2}}$
2	$\frac{4}{5} u_{eq} \left(\frac{B_{eq}}{B} \right)$	$\frac{1}{5} u_{eq} \left(\frac{B_{eq}}{B} \right)$
3	$\frac{5}{6} u_{eq} \left(\frac{B_{eq}}{B} \right)^{\frac{3}{2}}$	$\frac{1}{6} u_{eq} \left(\frac{B_{eq}}{B} \right)^{\frac{3}{2}}$

C. Response of the Magneto-ionospheric Plasma

In this section we show that the magneto-ionospheric plasma responds to the potential difference associated with a ring current energy density enhancement in the same way that a leaky capacitor responds to an applied potential difference. The time dependent polarization effects die away with a time constant that depends on the magneto-ionospheric plasma permittivity and on the ionospheric Pederson conductivity. The time constant for this decay varies with the sunspot cycle, with local time, and with the position of the enhancement in the magnetosphere.

We also show that the charge density that develops on the east and west boundaries of an energy density enhancement is much less than $n_{eq}q$, where n_{eq} is the equatorial number density of ring current particles within the enhancement.

The assumption that the magnetic field lines are equipotentials is equivalent to the assumption that the charges redistribute themselves "instantaneously" along the B lines. The polarization effects that give rise to a leaky capacitor time constant are due to motion of the plasma transverse to the field. In order to calculate the response of the magneto-ionospheric plasma we use the charge conservation equation appropriate to the equipotential field line approximation. That is, the equation of local conservation:

$$\frac{\partial \rho}{\partial t} + \text{div } \bar{j} = 0 \qquad \text{(locally)}$$

must be replaced by a volume integral:

$$\int_{\text{vol}} \left(\frac{\partial \rho}{\partial t} + \text{div } \bar{\jmath}\right) dv = 0 \quad , \qquad \qquad 28)$$

where the volume of integration is bounded by two planes of longitude separated by a small angle $\Delta\varphi$, two dipole shells separated by a small equatorial distance ΔR , and the earth's surface. In terms of the distance S_R along the field line, R , and θ , the volume integral is:

$$\int_{\Delta R} \int_{\Delta\varphi} \int_{\substack{\text{along} \\ \text{field} \\ \text{line}}} \left(\frac{\partial \rho}{\partial t} + \text{div } \bar{\jmath}\right) \frac{R \sin^6 \theta \ dS_R \ d\varphi \ dR}{\sqrt{1 + 3 \cos^2 \theta}} \quad .$$

In order that the above integral be identically zero, we require the inner integral to be zero:

$$\int_{\substack{\text{along} \\ \text{field} \\ \text{line}}} \left(\frac{\partial \rho}{\partial t} + \text{div } \bar{\jmath}\right) \frac{\sin^6 \theta \ dS_R}{\left(1 + 3 \cos^2 \theta\right)^{\frac{1}{2}}} = 0 \quad . \qquad \qquad 29)$$

Substituting:

$$\rho = \frac{\rho_{eq}}{\sin^6 \theta} \qquad \qquad 30)$$

and

$$\bar{j} = \bar{j}_G + \bar{j}_R + \bar{j}_P + \bar{j}_I \qquad \qquad 31)$$

into eq.(29), we have:

$$\frac{\partial}{\partial t}\left[\rho_{eq}\int \frac{dS_R}{\left(1 + 3\cos^2 \theta\right)^{\frac{1}{2}}}\right] = -\int \frac{\left(\bar{B} \times \overline{\nabla B}\right)}{B^3} \cdot \frac{\overline{\nabla u}_\perp \sin^6 \theta \; dS_R}{\left(1 + 3\cos^2 \theta\right)^{\frac{1}{2}}}$$

$$= -2\int \frac{\left(\bar{R}_c \times \bar{B}\right)\cdot\overline{\nabla u}_{\|} \sin^6 \theta \; dS_R}{R_c^2 B^2\left(1 + 3\cos^2 \theta\right)^{\frac{1}{2}}}$$

$$- \int \frac{div(\epsilon\bar{E}) \sin^6 \theta \; dS_R}{\left(1 + 3\cos^2 \theta\right)^{\frac{1}{2}}}$$

$$- \int \frac{div(\sigma_1\bar{E}) \sin^6 \theta \; dS_R}{\left(1 + 3\cos^2 \theta\right)^{\frac{1}{2}}} \; . \quad 32)$$

Assuming:

$$\bar{E} \cdot \overline{\nabla \epsilon} = \bar{E} \cdot \overline{\nabla \sigma_1} = 0 \quad ,$$

we have:

$$\text{div}(\epsilon \bar{E}) = \epsilon \frac{\partial(\bar{\nabla} \cdot \bar{E})}{\partial t} = \frac{\epsilon}{\epsilon_o} \frac{\partial \rho}{\partial t} = \frac{\epsilon}{\epsilon_o \sin^6 \theta} \frac{\partial \rho_{eq}}{\partial t} \quad ,$$

and

$$\text{div}(\sigma_1 \bar{E}) = \sigma_1 (\bar{\nabla} \cdot \bar{E}) = \frac{\sigma_1 \rho}{\epsilon_o} = \frac{\sigma_1}{\epsilon_o \sin^6 \theta} \rho_{eq} \quad .$$

The charge conservation equation [eq. (32)] may now be expressed in terms of the charge density in the equatorial plane:

$$\left[\int \frac{dS_R}{\left(1 + 3 \cos^2 \theta\right)^{\frac{1}{2}}} + \frac{1}{\epsilon_o} \int \frac{\epsilon \, dS_R}{\left(1 + 3 \cos^2 \theta\right)^{\frac{1}{2}}} \right] \frac{\partial \rho_{eq}}{\partial t}$$

$$+ \left[\frac{1}{\epsilon_o} \int \frac{\sigma_1 \, dS_R}{\left(1 + 3 \cos^2 \theta\right)^{\frac{1}{2}}} \right] \rho_{eq} + \Lambda = 0 \quad , \qquad 33)$$

where:

$$\Lambda = \Lambda_\perp + \Lambda_\parallel$$

$$= \int \frac{\left(\bar{B} \times \overline{\nabla B}\right) \cdot \overline{\nabla u}_\perp \sin^6 \theta \; dS_R}{B^3 \left(1 + 3 \cos^2 \theta\right)^{\frac{1}{2}}}$$

$$+ 2 \int \frac{\left(\bar{R}_C \times \bar{B}\right) \cdot \overline{\nabla u}_\parallel \sin^6 \theta \; dS_R}{R_C^{\;2} B^2 \left(1 + 3 \cos^2 \theta\right)^{\frac{1}{2}}} \quad . \tag{34}$$

Since $\epsilon \gg \epsilon_o$ throughout the magnetosphere (Figures 8 and 9), we have:

$$\int \frac{dS_R}{\left(1 + 3 \cos^2 \theta\right)^{\frac{1}{2}}} \ll \frac{1}{\epsilon_o} \int \frac{\epsilon \; dS_R}{\left(1 + 3 \cos^2 \theta\right)^{\frac{1}{2}}} \quad .$$

Hence, writing:

$$E \equiv \int \frac{\epsilon \; dS_R}{\left(1 + 3 \cos^2 \theta\right)^{\frac{1}{2}}} \tag{35}$$

and

$$\Sigma' \equiv \int \frac{\sigma_1 \ dS_R}{\left(1 + 3 \ \cos^2 \theta\right)^{\frac{1}{2}}} \tag{36}$$

eq.(33) becomes:

$$\frac{\partial \rho_{eq}}{\partial t} + \frac{\Sigma'}{E} \rho_{eq} \quad \frac{\epsilon_o \Lambda}{E} = 0 \quad . \tag{37}$$

The solution to eq.(37) is:

$$\rho_{eq}(t) = \rho_{eq}\left(e^{-t/\tau} - 1\right) , \tag{38}$$

where:

$$\rho_{eq} = \frac{\epsilon_o \Lambda}{\Sigma'} , \tag{39}$$

$$\tau = \frac{E}{\Sigma'} , \tag{40}$$

and

$$\rho_{eq}(t = 0) = 0 \qquad \text{is assumed .}$$

E has the units of capacitance (farads), and Σ' has the units of conductance (mhos). The equation expressing the build up of charge density with time [eq.(38)] is the leaky capacitor equation.

In order to evaluate ρ_{eq} and τ , it is necessary to estimate values for E and Σ' . In view of the scarcity of relevant magneto-ionospheric data and the large fluctuations known to occur in the pertinent parameters during magnetic storms, estimates based on extrapolation from low-latitude, idealized conditions must be regarded as tentative. Such, however, are the conditions on which the following estimates are based.

Above an altitude of $\approx$ 1500 km, hydrogen ions provide the main contribution to the magnetic plasma permittivity. The contribution of the hydrogen plasma to E may be calculated if one knows the distribution of the protons along a given field line. For example, we have plotted in Figure 8:

$$\frac{\epsilon_{H^+} R_E}{\left(1 + 3 \cos^2 \theta\right)^{\frac{1}{2}}} \quad vs \quad S_4 \quad \text{(in units of } R_E)$$

for the $R = 4R_E$ field line, assuming the background hydrogen plasma is in diffusive equilibrium at $T_e = T_p = 1250°K$ [Hanson (1965), p. 35]. Twice the area

under the curve in Figure 8 represents the contribution
of the hydrogen plasma to E . In this case the contri-
bution is ≈ 15 farads.

Below an altitude of about 1500 km, helium and
oxygen ions provide the main contribution to E . The
distribution of these ions, especially at high latitudes
is not well known. The contribution to ε from these
ions at a geomagnetic latitude of ≈ 30° is given in
Figure 9. Assuming the same distribution for these ions
at the base of the R = 4R_E field line, the contribution
to E ranges from ≈ 0.5 farads at night sunspot minimum
to ≈ 10 farads at day sunspot maximum.

Since σ_1 is a sharply peaked function of altitude,
we have:

$$\Sigma' = \frac{2}{\sin I} \frac{\Sigma_1}{\left(1 + 3 \cos^2 \theta\right)^{\frac{1}{2}}} = \frac{2\Sigma_1}{\sin I \left(4 - 3 \frac{R_E}{R}\right)^{\frac{1}{2}}} \quad ,$$

where:

$$\Sigma_1 = \int \sigma_1 dh = \text{the height integrated Pederson}$$
$$\text{conductivity,}$$

and

$$I = \text{the dip angle} \quad .$$

Since:

$$\sin I = \frac{2 \cot \theta}{\sqrt{1 + 4 \cot^2 \theta}} = \frac{2\sqrt{\frac{R}{R_E} - 1}}{\sqrt{\frac{R}{R_E}} \sqrt{4 - 3 \frac{R_E}{R}}} = \frac{2\sqrt{1 - \frac{R_E}{R}}}{\sqrt{4 - 3 \frac{R_E}{R}}}$$

we have:

$$\Sigma' = \frac{\Sigma_1}{\sqrt{1 - \frac{R_E}{R}}} \qquad . \qquad \qquad 41)$$

High-latitude values of Σ_1 , especially during magnetic storms, are poorly known. It is generally thought that the conductivity in the auroral regions is larger than the equatorial conductivity by about a factor of 5. The low-latitude quiet day values of Σ_1 can be obtained from Figure 3. These values range from ≈ 0.07 mhos for night sunspot-minimum to ≈ 25 mhos for day sunspot-maximum. Adopting these values for $\theta = 30°$, we have $\Sigma'_4 \approx 0.1$ mhos for night sunspot-minimum and $\Sigma'_4 \approx 30$ mhos for day sunspot-maximum.

According to these estimates, average (over the sunspot and local time cycles) values for E and Σ' for $R = 4R_E$ are:

$$E \approx 30 \text{ farads}$$

and

$$\Sigma' \approx 15 \text{ mhos.}$$

This gives an average value for the time constant of:

$$\tau \approx 2 \text{ seconds}.$$

We now show that the charge density at the boundaries of an energy density enhancement is much less than $n_{eq}q$, where n_{eq} is the equatorial number density of ring current particles. We make the cautious assumption that:

$$|\overline{\nabla u_\perp}| = \frac{u_\perp}{a_c} \text{,} \qquad\qquad 42)$$

and

$$|\nabla u_\parallel| = \frac{u_\parallel}{a_c} \text{,} \qquad\qquad 43)$$

where:

$$a_c = \frac{\sqrt{2m_p w}}{qB}$$

is the cyclotron radius for a proton with energy w (here w is the average energy of the proton energy density enhancement).

Using the fact that:

$$\left|\frac{\overline{\nabla_\perp B}}{B}\right| = \frac{1}{R_c} \text{,} \qquad\qquad 44)$$

we have:

$$\Lambda_\perp = \int \frac{(\bar{B} \times \overline{\nabla B}) \cdot \overline{\nabla u}_\perp \, \sin^6 \theta \, dS_R}{B^3 \left(1 + 3 \cos^2 \theta\right)^{\frac{1}{2}}}$$

$$= \int \frac{u_\perp \, \sin^6 \theta \, R \, \sin \theta \, d\theta}{R_c B a_c}$$

$$= \frac{3q}{\sqrt{2m_p w}} \int \frac{u_\perp \left(1 + \cos^2 \theta\right) \sin^6 \theta \, d\theta}{\left(1 + 3 \cos^2 \theta\right)^{3/2}} \qquad \cdot \qquad 45)$$

Similarly

$$\Lambda_{\parallel} = \frac{6q}{\sqrt{2m_p w}} \int \frac{u_{\parallel} \left(1 + \cos^2 \theta\right) \sin^6 \theta \, d\theta}{\left(1 + 3 \cos^2 \theta\right)^{3/2}} \qquad \cdot \qquad 46)$$

For the isotropic model ($\delta = 0$), we have:

$$\Lambda = \Lambda_{\parallel} + \Lambda_{\perp} = \frac{4q\, u_{eq}}{\sqrt{2m_p w}} \int \frac{\left(1 + \cos^2 \theta\right) \sin^6 \theta\, d\theta}{\left(1 + 3 \cos^2 \theta\right)^{3/2}}$$

$$< \frac{8q\, u_{eq}}{\sqrt{2m_p w}} \int_o^{\pi/2} \frac{\left(1 + \cos^2 \theta\right) \sin^6 \theta\, d\theta}{\left(1 + 3 \cos^2 \theta\right)^{3/2}}$$

$$< \frac{8q\, u_{eq}}{\sqrt{2m_p w}} \int_o^{\pi/2} 2 \sin^6 \theta\, d\theta$$

$$= \frac{16q\, u_{eq}}{\sqrt{2m_p w}} \left(\frac{5\pi}{32}\right)$$

$$= \frac{5\pi\sqrt{w}\, n_{eq}\, q}{2\sqrt{2m_p}}$$

$$= 1.7 \times 10^6 \sqrt{K}\, n_{eq}\, q \quad , \tag{47}$$

where:

      K =   the average proton energy in units of kev.,

and

      n_{eq} =   the equatorial proton number density.

We therefore find that an upper limit for ρ_{eq} is:

$$\rho_{eq} \; < \; \epsilon_o \frac{\Lambda}{\Sigma'} \; < \; 1.5 \times 10^{-6} \frac{\sqrt{K}}{\Sigma'} n_{eq} \; q \; . \quad (\delta = 0) \qquad 48)$$

A similar calculation for $\delta = 1, 2,$ and 3 shows that:

$$\rho_{eq} \; < \; 1.2 \times 10^{-6} \frac{\sqrt{K}}{\Sigma'} \; n_{eq} \; q \; , \qquad\qquad (\delta = 1) \qquad 49)$$

$$\rho_{eq} \; < \; 9.6 \times 10^{-7} \frac{\sqrt{K}}{\Sigma'} \; n_{eq} \; q \; , \qquad\qquad (\delta = 2) \qquad 50)$$

and

$$\rho_{eq} \; < \; 4 \times 10^{-7} \frac{\sqrt{K}}{\Sigma'} n_{eq} \; q \qquad . \qquad\qquad (\delta = 3) \qquad 51)$$

Since K and Σ' are of order 10, we conclude that $\rho_{eq} \; << \; n_{eq} \; q \; .$

FIGURE 8:   A plot of the integrand in the expression
for E . Twice the area under the curve
represents the contribution to the field
line integrated permittivity from hydrogen
ions along the $\frac{R}{R_E} = 4$ field line. In
deriving this curve diffusive equilibrium
at $T_e = T_p = 1250°\,K$ is assumed. The
curve was derived from the data of <u>Hanson</u>
(1965).

FIGURE 9:   The contribution to ϵ from helium and
oxygen ions at a geomagnetic latitude of
$\approx 30°$. These curves were derived from
data in <u>The Satellite Environment Handbook</u>
(1965).
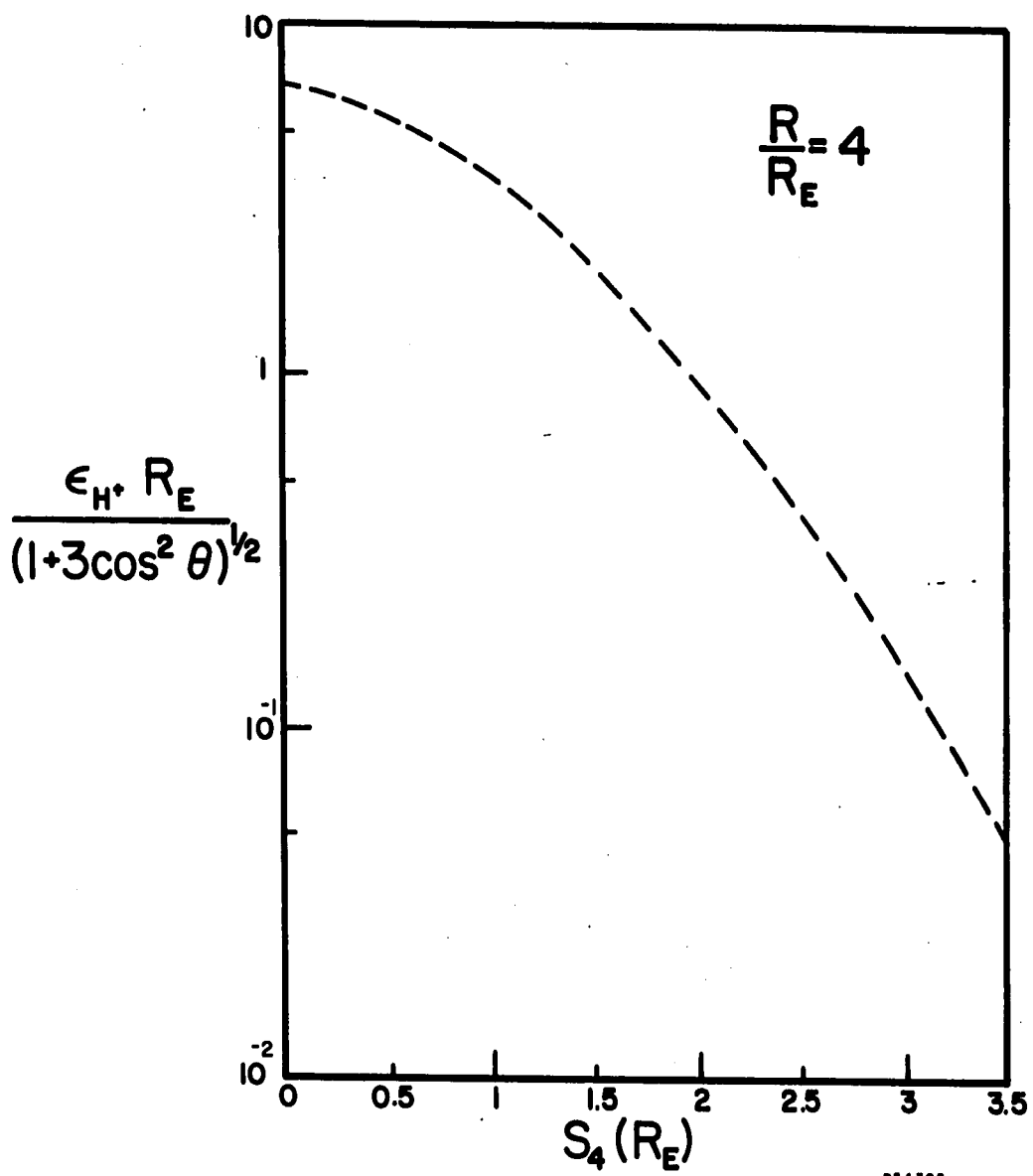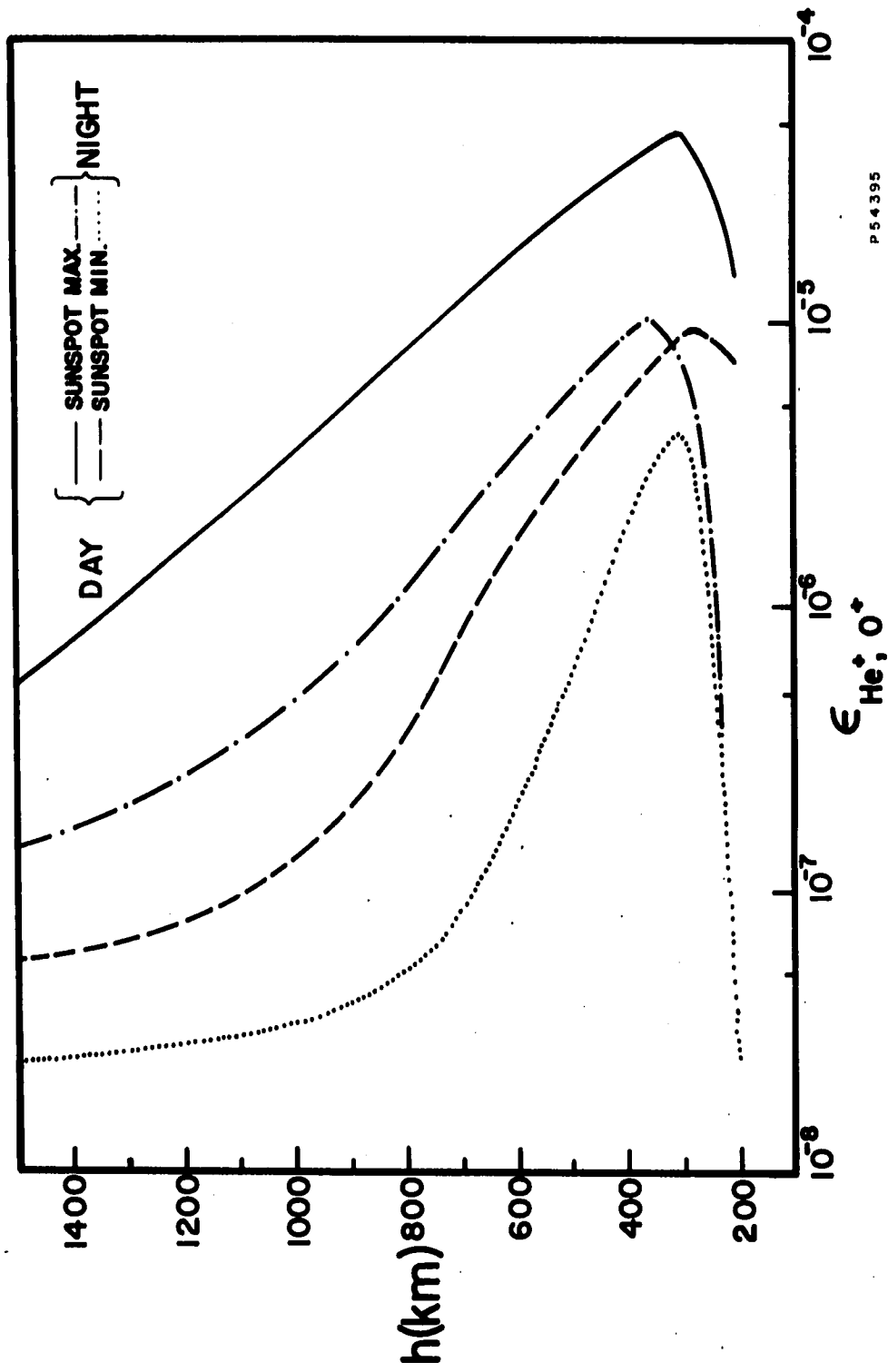
FIGURE 8

FIGURE 9

D. The Electric Drift Velocity of the Enhancement

As discussed briefly in the introduction, an energy density enhancement in the ring current belt tends to be ejected outward as viewed from the earth. In this section we show that all plasma along a given field line tends to move together. We derive an expression for the terminal electric field and electric drift velocity for a given enhancement. (By "terminal" we mean the electric field and drift velocity after the polarization effects have died away.)

The direction of the electric drift velocity is along curves of constant P, i.e., the orthogonal trajectories of the dipole field lines. The magnitude of the electric drift velocity at any point (r, θ) along a given dipole line is:

$$V_E = \frac{E_{eq}}{B_{eq}} \frac{\sin^3 \theta}{\sqrt{1 + 3 \cos^2 \theta}} \; . \qquad \qquad 52)$$

The time it takes for plasma initially at (r_1, θ_1) to go from the dipole field line characterized by R_1 to a dipole field line characterized by R_2 is:

$$\Delta T_{1,2} = \int \frac{dS_p}{V_E} = -\frac{P}{2} \frac{B_{eq}}{E_{eq}} \int_{\theta_1}^{\theta_2} \frac{\left(1 + 3 \cos^2 \theta\right)d\theta}{\sin^3 \theta \cos^{\frac{1}{2}} \theta}$$

$$= P \frac{B_{eq}}{E_{eq}} \left[\frac{\cos^{\frac{1}{2}} \theta_2}{\sin^2 \theta_2} - \frac{\cos^{\frac{1}{2}} \theta_1}{\sin^2 \theta_1} \right] . \qquad 53)$$

But by eqs.(9) and (10):

$$P \frac{\cos^{\frac{1}{2}} \theta_2}{\sin^2 \theta_2} = \frac{r}{\sin^2 \theta_2} = R_2 ,$$

and

$$P \frac{\cos^{\frac{1}{2}} \theta_1}{\sin^2 \theta_1} = R_1$$

Hence:

$$\Delta T_{1,2} = \frac{B_{eq}}{E_{eq}} (R_2 - R_1) , \qquad 54)$$

which is independent of P . Thus all plasma along a given field line tends to move together.

The statement "all plasma along a given field line tends to move together" is equivalent to the statement that the plasma is "tied" to the field lines. The tendency to move together is greater the lower the energy of the particles involved, since for high energy particles the electric drift velocity may not be the dominant drift velocity.

To calculate the electric field, and hence the electric drift velocity, associated with a given energy density enhancement, we use the fact that the charge density at the boundaries of an enhancement is always much smaller than q times the number density of ring current particles. Along a given line of magnetic force the sum of the currents associated with the current densities $\bar{j}_G$, $\bar{j}_R$, $\bar{j}_P$, and $\bar{j}_I$ is approximately zero:

$$\int_{\substack{\text{field} \\ \text{line}}} \left(\bar{j}_G + \bar{j}_R + \bar{j}_P + \bar{j}_I \right) dA = 0 \qquad 55)$$

or

$$\int \int \left(\bar{j}_G + \bar{j}_R + \bar{j}_P + \bar{j}_I \right) ds_R \, ds_P = 0 \qquad 56)$$

or by eq.(13):

$$\int\int \left(\bar{j}_G + \bar{j}_R + \bar{j}_P + \bar{j}_I\right) dS_R \; \frac{\sin^3 \theta \; dR}{\left(1 + 3 \cos^2 \theta\right)^{\frac{1}{2}}} \; = \; 0 \; . \quad 57)$$

Again we require the inner integral to be zero.
Hence :

$$\int \left(\bar{j}_G + \bar{j}_R + \bar{j}_P + \bar{j}_I\right) \frac{\sin^3 \theta \; dS_R}{\sqrt{1 + 3 \cos^2 \theta}} \; = \; 0 \quad 58)$$

or by eqs.(1), (2), (6), and (7):

$$\int \left(u_\perp \; \frac{\bar{B} \times \overline{\nabla B}}{B^3}\right) \frac{\sin^3 \theta \; dS_R}{\left(1 + 3\cos^2 \theta\right)^{\frac{1}{2}}} \; + \int 2u_\parallel \; \frac{\bar{R}_c \times \bar{B} \, \sin^3 \theta \; dS_R}{R_c^{\,2} B^2 \left(1 + 3 \cos^2 \theta\right)^{\frac{1}{2}}}$$

$$+ \int \frac{\left(\varepsilon \, \dot{\bar{E}} + \sigma_1 \bar{E}\right) \sin^3 \theta \; dS_R}{\left(1 + 3 \cos^2 \theta\right)^{\frac{1}{2}}} \; = \; 0 \; . \quad 59)$$

In terms of the electric field in the equatorial plane, we have by eqs.(21), (35), and (36):

$$\frac{\partial \bar{E}_{eq}}{\partial t} + \frac{\Sigma'}{E} \ \bar{E}_{eq} + \frac{\bar{J}}{E} = 0 \quad , \qquad\qquad 60)$$

where:

$$\bar{J}_\perp = \int \frac{u_\perp (\bar{B} \times \overline{\nabla B}) \sin^3 \theta \ dS_R}{B^3 \left(1 + 3 \cos^2 \theta\right)^{\frac{1}{2}}} \quad , \qquad\qquad 61)$$

$$\bar{J}_\| = \int \frac{2u_\| \ \bar{R}_c \times \bar{B} \sin^3 \theta \ dS_R}{R_c{}^2 B^2 \left(1 + 3 \cos^2 \theta\right)^{\frac{1}{2}}} \quad , \qquad\qquad 62)$$

and

$$\bar{J} = \bar{J}_\perp + \bar{J}_\| \quad . \qquad\qquad 63)$$

The solution for the equatorial electric field, assuming $\bar{E}_{eq} = 0$ at $t = 0$, is:

$$\bar{E}_{eq}(t) = \frac{\bar{J}}{\Sigma'} (e^{-t/\tau} - 1) = \bar{E}_{eq} (e^{-t/\tau} - 1) \quad , \qquad 64)$$

where again the time dependent polarization effects die away with the time constant:

$$\tau = \frac{E}{\Sigma'} \quad . \qquad\qquad 40)$$

The electric drift velocity is then given by:

$$\bar{v}_{E_{eq}}(t) = \frac{\bar{E}_{eq} \times \bar{B}_{eq}}{B_{eq}^2} = \frac{\bar{J} \times \bar{B}_{eq}(e^{-t/\tau} - 1)}{B_{eq}^2 \Sigma'} = \bar{v}_{E_{eq}}(e^{-t/\tau} - 1) . \quad 65)$$

The drift velocity at any point along the field line in question is simply related to the equatorial drift velocity, as discussed earlier in this section.

In the above expressions for the currents $\bar{J}_{\parallel}$ and $\bar{J}_{\perp}$, the energy densities $u_{\parallel}$ and $u_{\perp}$ refer to the enhancement in the ring current belt, i.e., not including the energy density of the uniform ring current belt. The currents can also be written:

$$\bar{J}_{\perp} = \int \frac{\Delta u_{\perp}(\bar{B} \times \overline{\nabla B}) \sin^3 \theta \, dS_R}{B^3(1 + 3 \cos^2 \theta)^{\frac{1}{2}}} , \quad 66)$$

and

$$\bar{J}_{\parallel} = \int \frac{2\Delta u_{\parallel}(\bar{R}_c \times \bar{B}) \sin^3 \theta \, dS_R}{R_c^2 B^2(1 + 3 \cos^2 \theta)^{\frac{1}{2}}} , \quad 67)$$

where:

$\Delta u_{\perp}$ and $\Delta u_{\parallel}$ represent the difference in the energy density of the enhancement and the energy density on either side of the enhancement.

Substituting eqs.(11), (20), and (44) into eqs.(66) and (67), we have:

$$J_\perp = \frac{6}{B_{eq}} \int_{\theta^*}^{\pi/2} \frac{\Delta u_\perp \sin^9 \theta \left(1 + \cos^2 \theta\right) d\theta}{\left(1 + 3 \cos^2 \theta\right)^2} \quad , \qquad 68)$$

and

$$J_{\parallel} = \frac{12}{B_{eq}} \int_{\theta^*}^{\pi/2} \frac{\Delta u_{\parallel} \sin^9 \theta \left(1 + \cos^2 \theta\right) d\theta}{\left(1 + 3 \cos^2 \theta\right)^2} \quad , \qquad 69)$$

where:

θ^* is the polar coordinate latitude of the tip of the energy density enhancement.

(If the particles within the tube of force containing the energy density enhancement are assumed to extend down to the surface of the earth, then $\theta^* = \theta_o$. Atmospheric absorption would attenuate the energy density enhancement near the earth's surface, so $\theta^* > \theta_o$.)

For the isotropic model we have:

$$J = J_\perp + J_\parallel = \frac{8\Delta u}{B_{eq}} \int_{\theta^*}^{\pi/2} \frac{\sin^9 \theta \left(1 + \cos^2 \theta\right) d\theta}{\left(1 + 3 \cos^2 \theta\right)^2} \quad . \quad 70$$

The integral:

$$\int_{\theta^*}^{\pi/2} \frac{\sin^9 \theta \left(1 + \cos^2 \theta\right) d\theta}{\left(1 + 3 \cos^2 \theta\right)^2}$$

$$= \int_0^{\sqrt{1 - \frac{R^*}{R}}} \frac{\left(1 - x^2\right)^4 \left(1 + x^2\right) dx}{\left(1 + 3x^2\right)^2} = G\left(\frac{R^*}{R}\right) \quad ,$$

where:

$$R^* = R \sin^2 \theta^*$$

is plotted in Figure 10. It has a constant value near 0.3 over a wide range of $\frac{R^*}{R}$.

Substituting $G\left(\dfrac{R^*}{R}\right) = 0.3$ in the expression for J , we have:

$$J = \frac{2.4\Delta u}{B_{eq}} \quad \text{amps/meter,} \qquad (\delta = 0) \qquad \text{71)}$$

hence:

$$E_{eq} = \frac{2.4\Delta u}{B_{eq}\Sigma'} \text{ volts/meter,} \qquad (\delta = 0) \qquad \text{72)}$$

and

$$v_{eq} = \frac{2.4\Delta u}{B_{eq}^2\Sigma'} \quad \text{meters/second.} \qquad (\delta = 0) \qquad \text{73)}$$

It is perhaps more useful to express the equatorial electric drift velocity in terms of β , the ratio of the particle energy density to the magnetic field energy density.

$$\beta_{eq} = \frac{u}{\left(B_{eq}^2/2\mu_o\right)} \quad , \qquad \text{74)}$$

Hence:

$$\Delta\beta_{eq} = \frac{\Delta u}{\left(B_{eq}^2/2\mu_o\right)} \quad , \qquad \text{75)}$$

and

$$V_{E_{eq}} = 9.6 \times 10^5 \frac{\nabla\beta_{eq}}{\Sigma'}$$

$$\approx \frac{\nabla\beta_{eq} \times 10^6}{\Sigma'} \quad \text{meters/second .} \quad (\delta = 0) \qquad 76)$$

We note here that the equatorial electric drift velocity is not seriously affected by the pitch angle distribution. For example, the drift velocity for $\delta = 2$ is:

$$V_{E_{eq}} = 7.3 \times 10^5 \frac{\nabla\beta_{eq}}{\Sigma'} \quad \text{meters/second.} \quad (\delta = 2) \qquad 77)$$

For the same total excess energy in a given flux tube, the electric drift velocities for different pitch angle distributions are almost equal. For example:

$$\left(V_{E_{eq}}\right)_{\delta = 2} = 1.05 \left(V_{E_{eq}}\right)_{\delta = 0} \qquad 78)$$

FIGURE 10:   A plot of:

$$G\left(\frac{R^*}{R}\right) = \int_0^{\sqrt{1 - \frac{R^*}{R}}} \frac{(1 - x^2)^4 (1 + x^2)\,dx}{(1 + 3x^2)^2}$$

$$= \int_0^{\pi/2} \frac{\sin^9 \theta\,(1 + \cos^2 \theta)\,d\theta}{(1 + 3\cos^2 \theta)^2}$$
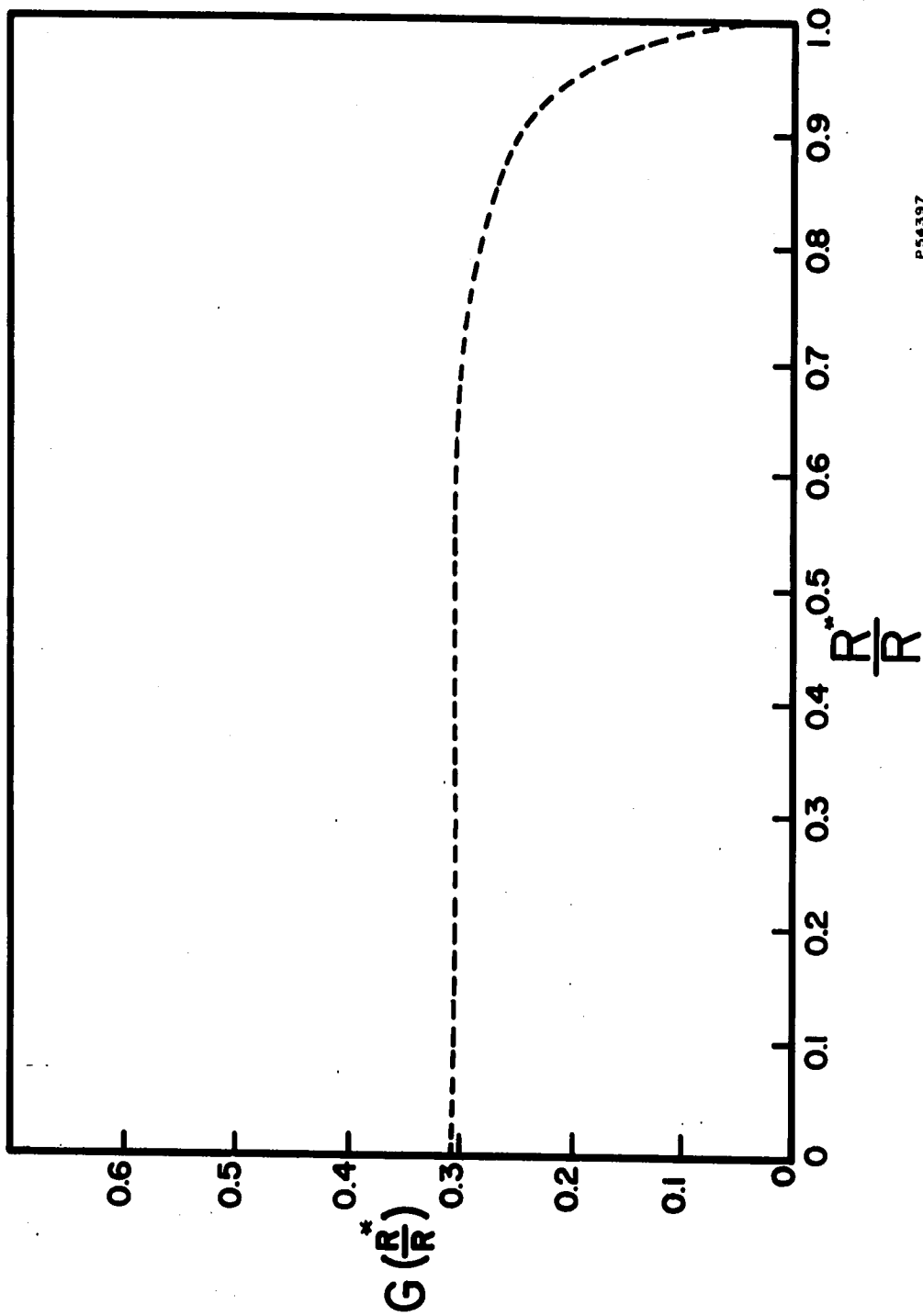
FIGURE 10

E. STABILITY AND ENERGETICS

The results of Sections C and D show that a non-uniform ring current belt tends to be stabilized by the conducting ionosphere. The equatorial ejection velocity associated with an energy density enhancement is inversely proportional to the height integrated Pederson conductivity.

In this section, we will discuss another stabilizing effect, caused by a spread in energies of the ring current particles. We will also examine the energetics of the problem and show that when a tube of flux containing an energy density enhancement is ejected from the ring current belt, most of the available particle energy is dissipated in the ionosphere.

Since the gradient and curvature drifts are energy dependent, an energy density enhancement that is not mono-energetic will tend to smear itself out. A crude indication of whether or not the electric drift velocity is large enough to overcome the stabilizing effect of a spread in energies in the enhancement is the ratio:

$$\frac{v_E}{v_D} \; .$$

where:

v_D is a characteristic longitudinal drift velocity for the enhancement.

If:

$$\frac{v_E}{v_D} \geq 1 \ ,$$

$$78)$$

then the energy density enhancement may be considered unstable.

If we define:

$$v_D = \frac{|\bar{j}|}{nq} \ ,$$

$$79)$$

then for the isotropic model, we have [eqs. (1),(2),(44); Table 1]:

$$v_D = \frac{4}{3} \frac{u}{nqR_cB} = \frac{4}{3} \frac{K \times 10^3}{R_cB} \ .$$

$$80)$$

The ratio $\frac{v_E}{v_D}$, evaluated in the equatorial plane is then [eqs. (77) and (80)]:

$$\left.\frac{v_E}{v_D}\right)_{eq} \approx \frac{5 \times 10^4 \ \Delta\beta_{eq}}{\Sigma' K R_o^2} \ .$$

$$81)$$

By evaluating the above ratio and comparing it with unity, one can estimate the stability of a given enhancement.

A value of $\beta \gtrsim 0.5$ is probably required to produce a main phase decrease of 100 γ . The exact value depends on the (presently unknown) distribution of the ring current particles in the magnetosphere. The quiet-time belt of low-energy protons ($E_p \gtrsim 100$ kev) reported by <u>Davis</u> and <u>Williamson</u> (1963) has a maximum value of $\beta \approx 0.25$ at $R = 3.5\ R_E$. These protons produce a magnetic field at the earth's equator of the order of 10 γ (<u>Akasofu</u>, <u>Cain</u>, and <u>Chapman</u>, 1961; <u>Hoffman</u> and <u>Bracken</u>, 1965).

Assuming ten per cent fluctuations in a ring current belt with $\beta_{eq} = 0.5$, we have:

$$\Delta\beta_{eq} = 0.05 .$$

Substituting:

$$\Sigma' = 15 \text{ mhos}$$

$$K = 10 \text{ kev}$$

and

$$R_o = 4$$

into eq. (81) gives:

$$\left.\frac{v_E}{v_D}\right)_{eq} \approx 1 . \tag{82}$$

This value is derived from an extrapolation of the quiet-day low-latitude conductivity. However it indicates that for cautious estimates of $\Delta\beta_{eq}$, a non-uniform ring current belt of 10 kev protons is only marginally stable. For the same values of $\Delta\beta_{eq}$ and R_o the stability of the ring current belt increases with the average particle energy. For the same values of $\Delta\beta_{eq}$ and K the stability increases with decreasing geocentric radial distance to the ring current belt. We note also that since the night time values of the height integrated Pederson conductivity may be lower than the day values by as much as a factor of 50, the night side of a non-uniform ring current belt should be less stable than the day side.

Provided the ejection is slow enough, the magnetic-moment and bounce actions of the ring current particles are conserved. In this case, the energy of the particles within the enhancement decreases in a way that is subject to calculation (e.g., Nakada et al., 1965). In particular, for particles that mirror in the equatorial plane the particle energy decreases with the cube of the geocentric distance to the tube of flux. The decrease in particle energy for other pitch angles is less severe, but still considerable (see Figure 7).

The energy made available by the adiabatic ejection of a flux tube containing ring current particles may be channeled in two directions. It can appear as kinetic energy of electric drift motion or it may be dissipated in the ionosphere as Joule heating from the ionospheric currents.

In the limiting case of high ionospheric conductivity the ejection velocity of a flux tube is low, and most of the available ring current-particle energy is dissipated in the ionosphere. For low ionospheric conductivities the ejection velocity is high, and most of the available energy appears as kinetic energy of electric drift motion.

The kinetic energy due to electric drift motion within a given tube of flux is:

$$\int_{\Delta R} \int_{\Delta\varphi} \int_{S_R} \tfrac{1}{2}\rho v_E^{\,2}\,dv = \int_{\Delta R} \int_{\Delta\varphi} \int_{S_R} \tfrac{1}{2}\rho \frac{E^2}{B^2} \frac{\sin^6\theta\; R\; dS_R\; d\varphi\; dR}{\left(1 + 3\cos^2\theta\right)^{\frac{1}{2}}}$$

$$= \int_{\Delta R} \int_{\Delta\varphi} \int_{S_R} \frac{\tfrac{1}{2}\epsilon\, E_{eq}^2\; dS_R\; d\varphi\; R\; dR}{\left(1 + 3\cos^2\theta\right)^{\frac{1}{2}}} \quad,$$

or,

$$\int_{\Delta R} \int_{\Delta\varphi} \int_{S_R} \tfrac{1}{2}\rho v_E^{\,2}\,dv = \int_{\Delta R} \int_{\Delta\varphi} \tfrac{1}{2}\, E\, E_{eq}^2\; R\; d\varphi\; dR \quad . \qquad 83)$$

On the other hand the energy of the ring current particles themselves, i.e., the kinetic energy of circulatory motion, is given by:

$$\int_{\Delta R} \int_{\Delta \varphi} \int_{S_R} u\, dv \;=\; \int_{\Delta R} \int_{\Delta \varphi} \int_{S_R} \frac{u \sin^6 \theta \; dS_R \; d\varphi \; dR}{\left(1 + 3 \cos^2 \theta\right)^{\frac{1}{2}}} \; . \qquad 84)$$

For the isotropic model, u is constant along a line of force, hence:

$$\int_{\Delta R} \int_{\Delta \varphi} \int_{S_R} u\, dv \;=\; \int_{\Delta R} \int_{\Delta \varphi} u R^2 \int_{\theta^*}^{\pi-\theta^*} \sin^7 \theta \; d\theta \; d\varphi \; dR \; .$$

The integral:

$$\int_{\theta^*}^{\pi-\theta^*} \sin^7 \theta \; d\theta \;=\; H\left(\frac{R^*}{R}\right)$$

is plotted in Figure 11. As can be seen from this figure, $H\left(\frac{R^*}{R}\right)$ is fairly constant over a wide range of $\frac{R^*}{R}$, having the value ≈ 0.45.

Setting:

$$H\left(\frac{R^*}{R}\right) = 0.45 \quad ,$$

we have:

$$\int_{\Delta R}\int_{\Delta\varphi}\int_{S_R} u\,dv = \int_{\Delta R}\int_{\Delta\varphi} [0.45\ uR]\,R\,d\varphi\,dR \quad . \qquad 85)$$

We can estimate the relative importance of the two channels for the available ring current energy by comparing the integrands of eqs. (83) and (85):

$$\tfrac{1}{2}\,E\,E_{eq}^2$$

and

$$0.45\ uR \approx \tfrac{1}{2}\ uR \quad .$$

If:

$$E\,E_{eq}^2 \ll uR \quad , \qquad 86)$$

then most of the ring current belt energy is dissipated in the ionosphere. On the other hand, if:

$$E\,E_{eq}^2 \approx uR \quad , \qquad 87)$$

then most of the ring current belt energy is being
converted into kinetic energy of electric drift motion.
This interpretation becomes particularly clear when
one considers that:

$$E \quad \text{corresponds to} \quad R\epsilon \;=\; \frac{R\rho}{B^2} \quad ,$$

hence:

$$E\,E^2 \quad \text{corresponds to} \quad R\rho\,\frac{E^2}{B^2} \;=\; R\rho v_E^2$$

$$=\; 2\,R\!\left(\tfrac{1}{2}\rho v_E^2\right) \quad .$$

Substituting:

$$E \;=\; 30 \text{ farads}$$

and

$$E^2_{eq} \;=\; B^2_{eq}v^2_{E_{eq}} \qquad\qquad \text{[eq. (52)]}$$

$$\approx\; B^2_{eq}v^2_{D_{eq}} \qquad\qquad \text{[eq. (82)]}$$

$$\approx\; B^2_{eq}\left(\frac{4}{3}\frac{K\times 10^3}{R_c B}\right)^2_{eq} \qquad \text{[eq. (80), } \delta = 0]$$

$$=\; \frac{K^2\times 10^6}{R_E^2} \quad , \qquad\qquad [R_o = 4]$$

we find for $K = 10$:

$$E\ E_{eq}^2 \approx 8 \times 10^{-5}\ . \qquad [\delta = 0,\ R_o = 4,\ K = 10]$$

For 10 kev protons with a number density of $10^7/m^3$ at $R_o = 4$, we have:

$$uR \approx 4 \times 10^{-1}\ .$$

Hence, these estimates indicate:

$$E\ E_{eq}^2 \ll uR\ .$$

For night sunspot minimum conditions, the electric drift velocity may be larger than we have assumed. However, unless:

$$\frac{v_E}{v_D} \approx 100\ ,$$

we may assume that most of the available ring current energy is dissipated in the ionosphere.

In this section we have argued that, in order for the ejection process to be important, the energy density enhancement must satisfy a local instability criterion:

$$\frac{v_E}{v_D} \geq 1\ . \qquad\qquad\qquad 78)$$

We use the word "local" because the ring current belt parameters (and the ionospheric conductivity) may change with geocentric distance (geomagnetic latitude) and thus change the value of v_E/v_D . For example, the background ring current belt energy density may not decrease sufficiently rapidly with geocentric distance to allow the instability criterion to be satisfied throughout the belt.

The reason for this is most easily seen from the hydromagnetic point of view rather than from the point of view of single-particle-orbit theory (c.f. Gold, 1959; Sonnerup and Laird, 1963). From this point of view, the instability is important if it is energetically possible for two tubes of flux, separated in radial distance, to interchange. Since the particle energy decreases roughly as R^{-3} and the volume of a tube of flux increases as R^4 , we see that unless the energy density of the ring current belt decreases faster than $\sim R^{-7}$, the interchange of flux tubes is energetically impossible.

From these considerations, we see that the instability is most likely to be important at the outer boundary of the ring current belt, where a sharp negative gradient in the energy density could be present. A sharp field-aligned gradient in the equatorial profile of both the electron (Carpenter, 1963) and positive-ion (Taylor et al., 1965) background plasma has been observed. It is not yet known if this "boundary" in the background plasma corresponds to a "boundary" in the ring current belt.

FIGURE 11:   The integral:

$$\int_{\theta^*}^{\pi - \theta^*} \sin^7 \theta \ d\theta \ = \ H \left(\frac{R^*}{R} \right) \ .$$

FIGURE II

P54398

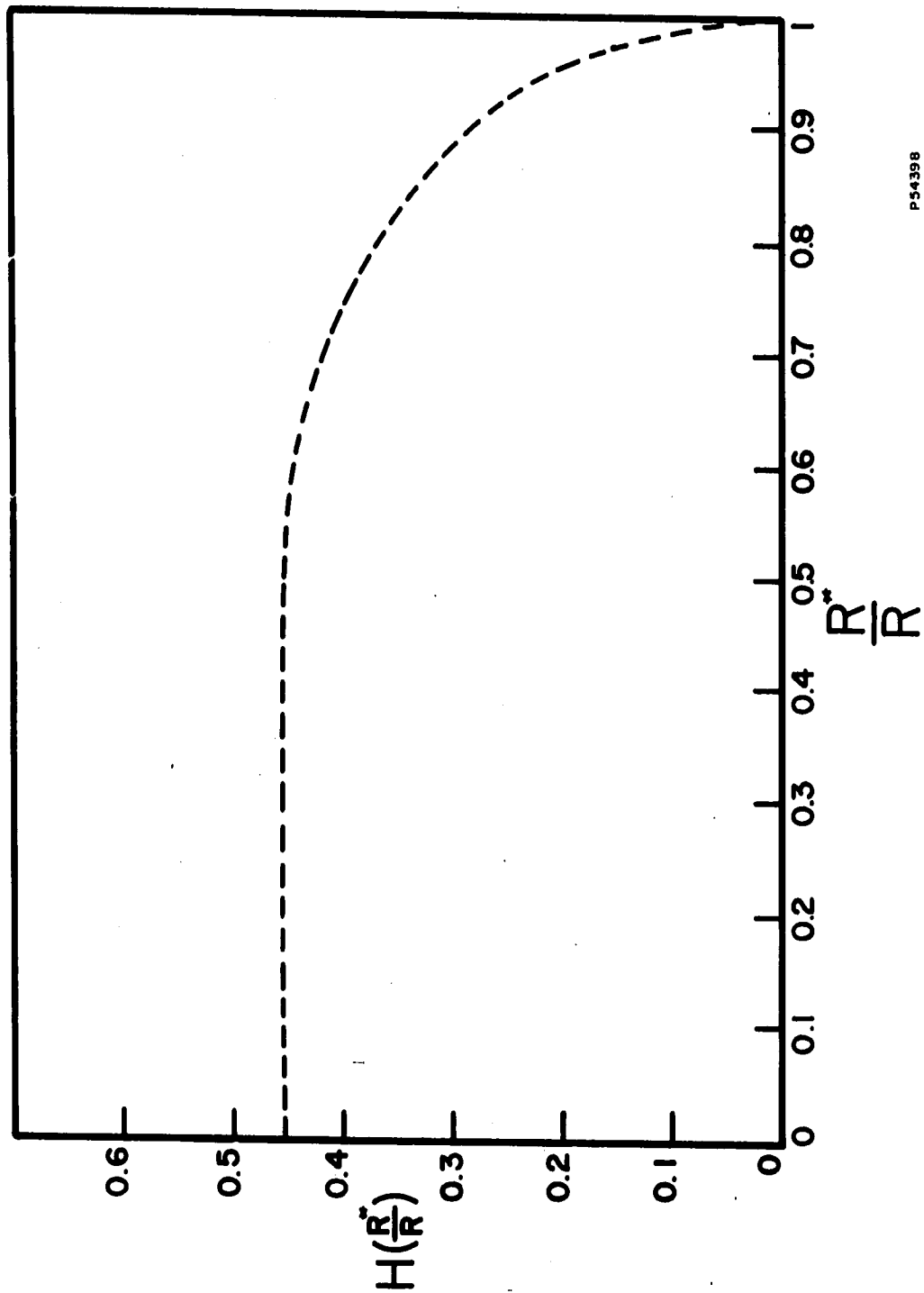## F. APPLICATION TO IONOSPHERIC HEATING

In Section E we have argued that the energy of the ejected ring current particles is likely to be dissipated in the ionosphere via Joule heating of the Pederson current. In this section we examine the possibility that the non-uniform ring current belt model could account for the magnetic storm associated phenomenon of ionospheric heating. We estimate the power input into the ionosphere caused by the Joule heating of the stabilizing currents associated with a non-uniform ring current belt, and compare this power input with that caused by EUV (Extreme Ultraviolet Light). We show that if the recovery of a magnetic storm is a result of the proposed transfer of ring current particle energy to the ionosphere, the power input is $\sim 10^{11}$ watts. This value is about a factor of ten less than the estimated power input caused by absorption of solar EUV, $\sim 10^{12}$ watts (Hunt and Van Zandt, 1961; Harris and Priester, 1963).

It has been shown that the temperature variations of the upper atmosphere are correlated with geomagnetic activity as measured by the a_p index (Jacchia, 1961 a,b). Several mechanism have been discussed that relate to this phenomenon, including heating due to the dissipation of hydromagnetic wave energy (Dessler, 1959; Karplus et al., 1962), magnetic storm related heating by internal atmospheric gravity waves (Hines, 1965), and Joule heating from ionospheric currents (Cole, 1961).

Cole (1961) calculated the ionospheric heating rate
from estimates of the ionospheric currents and conducti-
vities. If the non-uniform ring current belt is a valid
model, it is possible to take a different approach in
calculating the ionospheric heating rate. In the non-uniform
ring current model the decrease in energy content of the
ring current belt appears as heat energy in the ionosphere.
The ionospheric heating rate is given by:

$$\frac{dQ_I}{dt} = - \frac{dU_{RC}}{dt} \qquad \qquad 88)$$

where:

$$Q_I = \text{heat input into the ionosphere,}$$

and

$$U_{RC} = \text{energy content of the ring current belt.}$$

But, as pointed out by Dessler and Parker (1959),
the energy content of the ring current belt is related to
the magnetic field decrease, - B_{RC} , produced at the
earth's equator by the expression:

$$U_{RC} = - \frac{2}{3} \frac{B_{RC} U_m}{B_o} \qquad \qquad 89)$$

where:

$$U_m = 8 \times 10^{17} \text{ joules is the total geomagnetic field energy external to the earth,}$$

and

$$B_o = 3 \times 10^{-5} \text{ webers/m}^2 \text{ is the field strength at the earth's equator.}$$

Using this relation, the power input into the ionosphere may be calculated as a function of $\frac{dB_{RC}}{dt}$, the rate of change of the ring current magnetic field as measured at the earth's equator:

$$P_I = \frac{dQ_I}{dt} = 1.8 \times 10^{22} \frac{dB_{RC}}{dt} \text{ watts.} \qquad 90)$$

For a main phase decrease of 100 γ that recovers in $\sim 3.6 \times 10^4$ seconds (10 hours), we have:

$$\frac{dB_{RC}}{dt} \approx 2.8 \times 10^{-10} \text{ webers/m}^2 \text{ sec },$$

hence:

$$P_I \approx 0.5 \times 10^{11} \text{ watts }. \qquad 91)$$

This power input is less than the estimates of the power input due to EUV, $\sim 10^{12}$ watts, (Harris and Priester, 1963; Hunt and Van Zandt, 1961). In order to account for the temperature variations of the upper atmosphere during magnetic storms the power input must be somewhat above the average EUV value. We note however that the above estimate of the power input into the ionosphere is a lower bound to the actual Joule heating rate during a magnetic storm. The estimate is only appropriate for the recovery phase and cannot take into account Joule heating during the active part of the main phase.

ASYMMETRIC RING CURRENTS

A. THE LOW-LATITUDE DISTURBANCE-DAILY VARIATION

As discussed in the Introduction, the low-latitude
disturbance-daily variation is presently unexplained.
Some authors have argued that the local time dependence
of the storm field implies that most of the source currents
are in the ionosphere (Vestine, 1953; Sugiura, 1953). The
Chapman S_D current system (Chapman and Bartels, 1940,
p. 302) or some variation of this current system, repre-
sents an attempt to explain the local time dependence in
this way. However, Akasofu and Chapman (1964) have argued,
using high- and low-latitude magnetic data, that the low-
latitude disturbance-daily variation cannot be attributed
to the equatorward extension of a polar ionospheric current
system. By a detailed study of several large storms,
Akasofu and Chapman showed that the main phase storm field
can be asymmetric even when there are no significant
ionospheric currents flowing in the polar regions.

In this part of the thesis an extension of the
symmetric ring current model is described that could account
for the low-latitude disturbance-daily variation. The pro-
posed extension is simply that the main phase ring current
belt is asymmetric, having a larger energy content on the
evening side than on the morning side of the earth.

In order to check the proposed explanation for the
low-latitude disturbance-daily variation, a mathematical
model of an asymmetric ring current is developed. Asymmetric

ring current functions are derived that give the magnetic effects that would be observed by a low-latitude station as it rotates beneath an asymmetry in an otherwise uniform ring current belt. Allowance is made in the mathematical model for the drift of the asymmetry in local time and for the recovery in universal time of both the symmetric ring current and the asymmetry in the ring current belt.

Recovery phases for stations with various longitudes are derived and compared with measured recovery phases for a few magnetic storms. The comparisons show that even a very simple model of the asymmetric ring current can account for most of the low-latitude disturbance-daily variation.

B. THE ASYMMETRY IN THE STORM FIELD

The low-latitude disturbance-daily variation is a
result of an asymmetry in the main phase storm field. The
asymmetry is generally east-west, as can be seen from
Figure 12. In each of the polar histograms shown in Figure
12, the frequency of occurrence of an event is plotted
against local time. An "event" occurs whenever the hourly
averaged value of H falls below its monthly 5-quiet-day
average by more than 100 γ . Five years of data (1957-1961)
were used to make these histograms for Honolulu, San Juan,
Tucson, and Fredericksburg. By defining zero for each hour
of local time as the 5-quiet-day values, we have attempted
to subtract the quiet-day daily variation from the distur-
bance-daily variation in H.

The first thing to note about Figure 12 is that the
histograms are of the same form for Honolulu (geomagnetic
latitude λ_m = 21.1°), San Juan (λ_m = 29.9°), and Tucson
(λ_m = 40.4°). The maximum frequency of occurrence of events
($|\Delta H| \geq 100$ γ) is centered about 1800 hours for each of
these low latitude stations. There is a decrease in the
total number of events with increasing geomagnetic latitude.
If the storm field lines are roughly perpendicular to the
equatorial plane, one expects this decrease since H repre-
sents the projection of the storm field on the local north-
south horizontal.

The second thing to notice about the histograms of
Figure 12 is the sudden change in form at Fredericksburg
(λ_m = 49.6°). For Fredericksburg, this histogram

representation of the disturbance-daily variation is not
very appropriate because it presents only part of the
effect. At high latitude stations, large positive excur-
sions of H occur. A more appropriate representation of
the high-latitude disturbance-daily variation is given by
Chapman and Bartels (1940, p. 277 ff.). Chapman illus-
trated the disturbance-daily variation by deriving an
average storm from some 40 storms and then comparing each
individual storm with the average storm to derive a local
time dependence.

Presumably, the local time dependence of the storm
field at magnetic stations with $\lambda_m \geq 45°$ is due primarily
to ionospheric currents. Some of these ionospheric
currents may be associated with the asymmetric ring current
belt, as we will discuss briefly below.

FIGURE 12: A polar histogram showing as a function
of local time the frequency with which
$(H_{5\text{ quiet day}} - H) \geq 100\ \gamma$. This figure
shows all data from Honolulu (magnetic
latitude $\lambda_m = 21.1°$), San Juan ($\lambda_m = 29.9°$),
Tucson ($\lambda_m = 40.4°$), and Fredericksburg
($\lambda_m = 49.6°$), for the years 1957 through
1961.
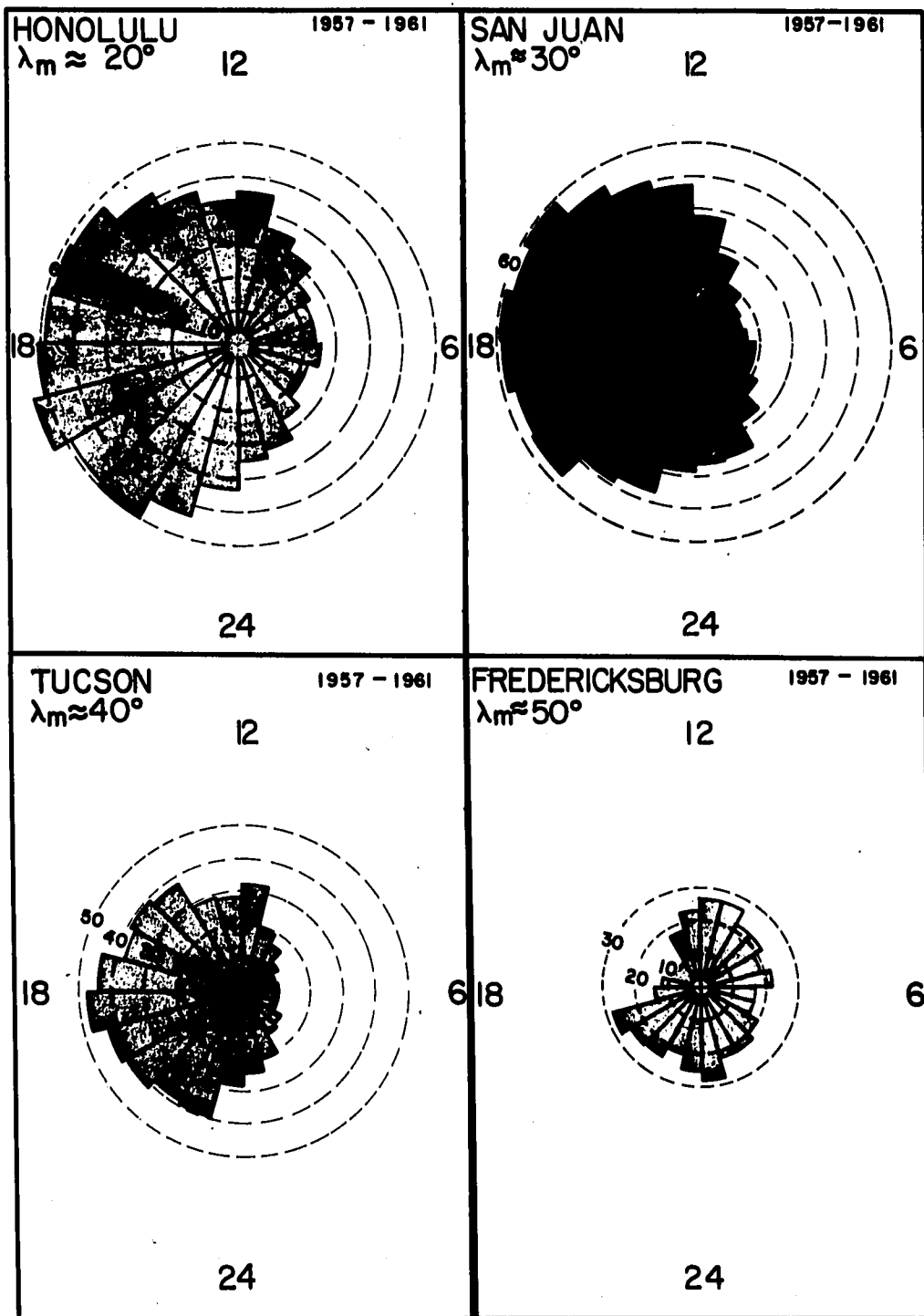
Figure 12

C. THE PARTIAL RING CURRENT SYSTEM

An asymmetric ring current is equivalent to a symmetric ring current plus a superimposed partial ring current system. The current system for the partial ring current, proposed earlier by Fejer (1961), is shown in Figure 13. In this figure the shaded region represents the asymmetry in an otherwise uniform ring current belt. The current in the equatorial element of the partial ring current system is due to the gradient and curvature drift motion of the charged particles that make up the asymmetry. The current flowing along the earth's field lines is carried by the low energy background plasma of the magnetosphere.

Not shown in Figure 13 are the Hall currents that flow in the ionosphere around the points of entry and exit of the current carrying field lines in the partial ring current system (c.f. Fejer, 1961). The magnetic fields of the Hall currents associated with the partial ring current system are important for high latitude stations. However, in this thesis we restrict our attention to low-latitude stations and neglect the magnetic effects of the Hall currents.

As a station rotates beneath the asymmetry, the value of H decreases below the symmetric ring current value. Note that an equatorial station beneath the asymmetry is, in effect, midway between two current loops, the upper and lower portions of the partial ring current system. Each

current loop carries current I/2 circulating clockwise
as viewed from above the north pole.

All charged particles in the magnetosphere tend to
co-rotate with the earth, so the asymmetry in the ring
current belt will not in general remain fixed in local
time. Protons have a westward gradient and curvature
drift velocity and electrons drift eastward. Hence, the
net drift of the asymmetry in local time can either be
eastward or westward depending on the particle type, energy
distribution, and geocentric distance of the ring current
particles. For example, 10 kev protons between $R = 3R_E$
and $R = 4R_E$ drift westward with a drift rate of
approximately 0.3 hours in local time per hour of univer-
sal time. (Note the drift rate in a non-rotating magne-
tosphere would be 1.3 hours in local time per hour of
universal time.) The eastward drift rate for 10 kev
electrons at the same geocentric distance is approximately
2.3 hours in local time per hour of universal time.

FIGURE 13:　　　　　The partial ring current system. The

current flowing along the field lines is

carried by the low energy background

plasma of the magnetosphere. The current

in the equatorial segment arises from the

drift motion of the ring current particles.

Note that an equatorial magnetic station

is, in effect, midway between two current

loops, each carrying current I/2 circu-

lating in the clockwise direction as

viewed from above the north pole. The

current loops are parallel in the equa-

torial plane giving the current I in the

equatorial segment of the partial ring

current system.

N
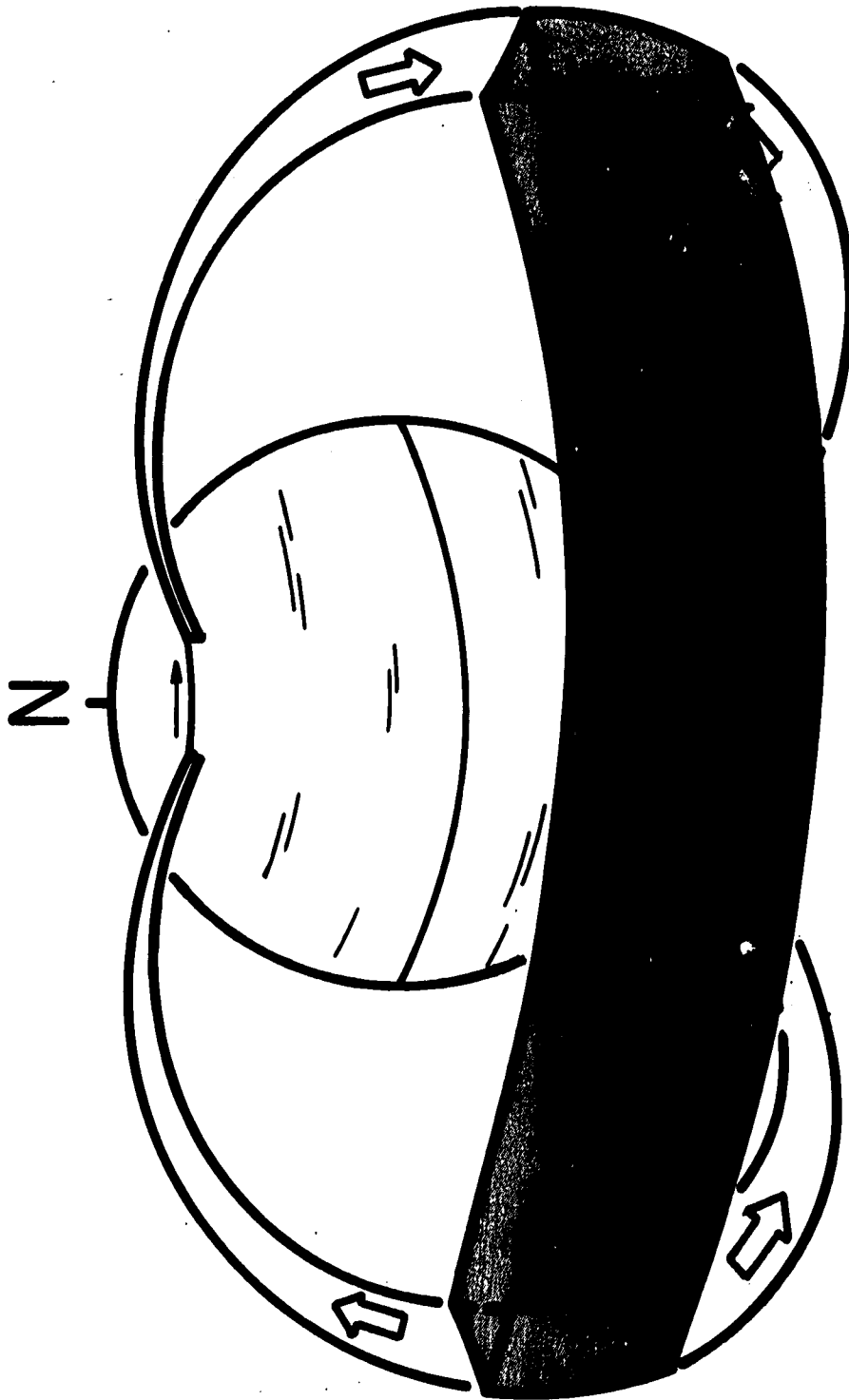
P54400

FIGURE 13

D. THE MATHEMATICAL MODEL

In this section we describe the mathematical model used to simulate the physical model of an asymmetric ring current.

In order to compute the partial ring current functions, a wire model of the current system was built to serve as an analog computer. In the model, sketched in Figure 14, the geocentric distance to the equatorial element was scaled to 4 earth radii. The dipole loops of the current model were connected in the "polar" region with copper braid so that the angle, ψ , between the two dipole loops could be easily varied.

Measurements of the model partial ring current field were made with a small flux gate magnetometer. The magnetometer was perpendicular to the equatorial plane of the scale model at a distance corresponding to one earth radius. The partial ring current functions were derived by sampling the magnetic field at various longitudes.

The derived partial ring current functions are shown in Figure 15. The angle characterizing each function corresponds to the separation angle between the two dipole arms of the current system. The abscissa for these functions is longitude expressed in hours (1 hour corresponds to 15°) from φ_o , the local time about which the partial ring current is centered. The partial ring current is assumed fixed in local time and each function is normalized to - 1.0 at φ_o .

Note that at those local times opposite to φ_o, the partial ring current actually provides a slight positive contribution to the storm field. The magnetic effect of the current along the dipole arms outweighs the effect of the equatorial segment for these hours.

In order to simulate the recovery of magnetic storms, we assume the partial ring current decays exponentially. That is, if $P_\psi(\varphi)$ denotes one of the partial ring current functions shown in Figure 15, then:

$$P_\psi(\varphi, t) = P_\psi(\varphi) \exp(-t/\tau_p) , \qquad\qquad 92)$$

where:

$$\tau_p = \text{the time constant for decay of the partial ring current.}$$

In addition to the partial ring current, we assume a symmetric ring current that also decays exponentially. We have:

$$S(t) = -S \exp(-t/\tau_s) , \qquad\qquad 93)$$

where:

$$\tau_s = \text{the time constant for decay of the symmetric ring current,}$$

and

S　　= the amplitude of the symmetric ring
current, i.e., $-S$ is the symmetric
part of the decrease in H observed
at the equator at the beginning of
the recovery phase.

We take account of the movement of the partial ring
current in local time in the following way. Suppose the
partial ring current is initially (i.e., at the beginning
of the recovery phase) centered about some longitude φ_o ,
and that it subsequently moves in local time with a
constant angular velocity $\dot{\varphi}$. At a later time t , the
partial ring current is centered about the longitude:

$$\varphi = \varphi_o - \dot{\varphi}t$$

where $\dot{\varphi}$ is positive if the partial ring current drifts
westward in local time. The magnetic effect observed at
an equatorial station with longitude φ_x is given by:

$$\Delta H = A \, P_\psi(|\varphi - \varphi_x|, \, t) + S(t) \quad ,$$

or,

$$\Delta H = A\, P_y\Big(|\varphi - \varphi_x|,\ t\Big) + S(t)$$

$$= A\, P_y\Big(|\varphi_0 - \dot\varphi t - \varphi_x|\Big)\ \exp(-t/\tau_p)$$

$$-S\ \exp(-t/\dot\tau_S)$$

$$= A\, P_y\Big(|\varphi_0 - \varphi_{x0} - (\dot\varphi + 1)t|\Big)\ \exp(-t/\tau_p)$$

$$-S\ \exp(-t/\tau_S)\ ,\hspace{3cm} 94$$

where:

A = the amplitude for the partial ring
current, i.e., -A is the asymmetric part
of the decrease in H observed at an
equatorial station directly beneath the
center of the partial ring current at
the beginning of the recovery phase.

Finally, we try to account for the geomagnetic
latitude, λ_x , of station x by multiplying eq. (94)
by $\cos \lambda_x$. That is:

$$\Delta H(\varphi_{x0}, \lambda_x, t) = \cos \lambda_x \left\{ A\, P_y\Big(|\varphi_0 - \varphi_{x0} - (\dot\varphi + 1)t|\Big) \cdot \right.$$

$$\left. \exp(-t/\tau_p) - S\ \exp(-t/\tau_p)\right\}\ .\hspace{2cm} 95)$$

The physical model under consideration represents a simple, idealized extension of the uniform ring current hypothesis. We have assumed there is no structure in the uniform ring current belt except for a single uniform enhancement spanning a large angle.

The mathematical model we have developed only approximates the physical model under consideration. There is provision in the model for the size of the partial ring current and for its drift in local time. There is little or no provision, however, for:

1) the change in size with time, e.g., the smearing out of the partial ring current in time, although the time constant τ_p may partially take account of this effect,

2) possible changes in local time drift rate,

and 3) the change in radial position of the partial ring current with time; in fact, the radial position of the partial ring current is fixed at $R = 4R_E$ in the model. Again, the time constant τ_p may partially account for the outward radial drift and consequent de-energization of the asymmetry.

FIGURE 14:   A sketch of the wire model used as an
              analog computer to calculate the partial
              ring current functions.

FIGURE 15:   Three partial ring current functions
              corresponding to separation angles between
              the dipole arms of the partial ring current
              system of 100°, 140°, and 180°.
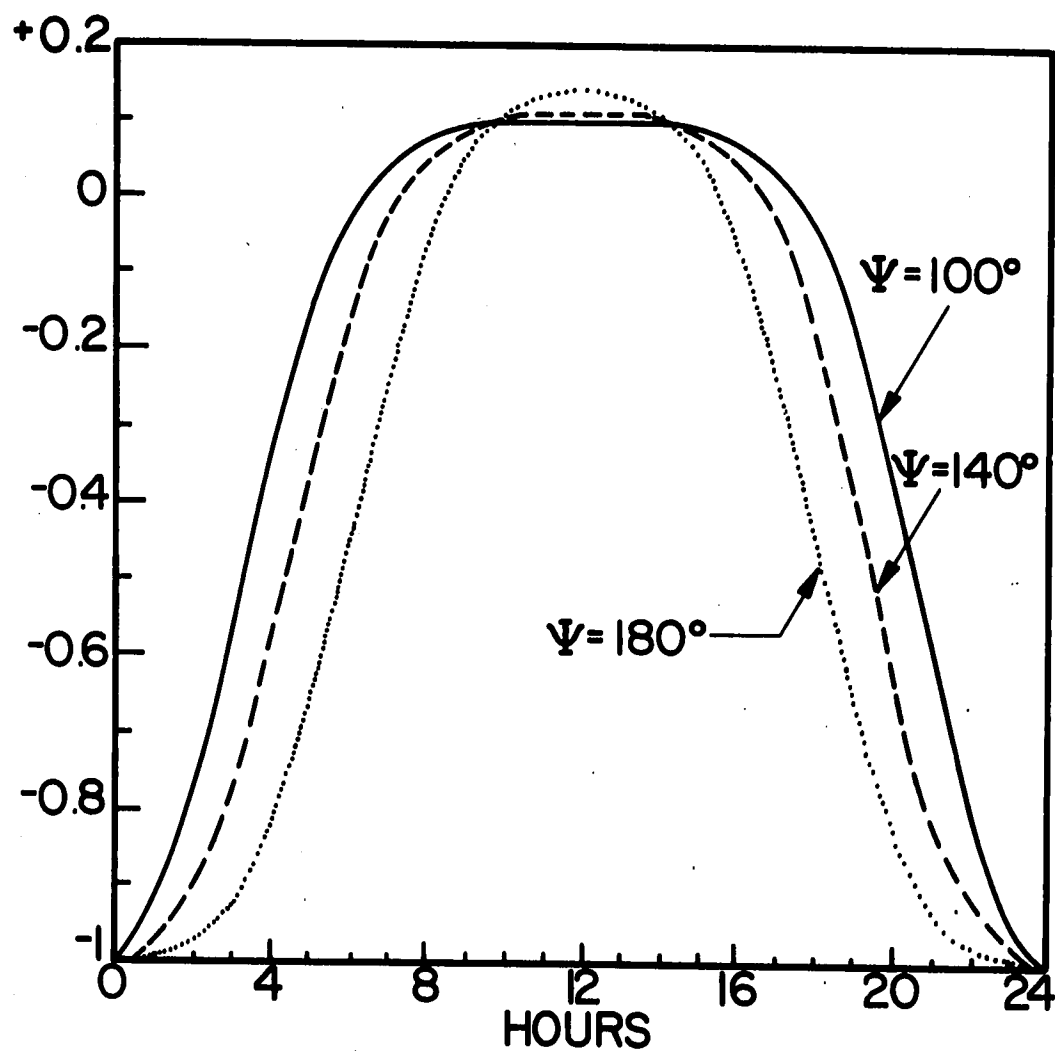
TO CURRENT
SOURCE

$\frac{I}{2}$

$\frac{I}{2}$

I

40 cm

MAGNETOMETER

N

S

I

$\frac{I}{2}$

$\frac{I}{2}$
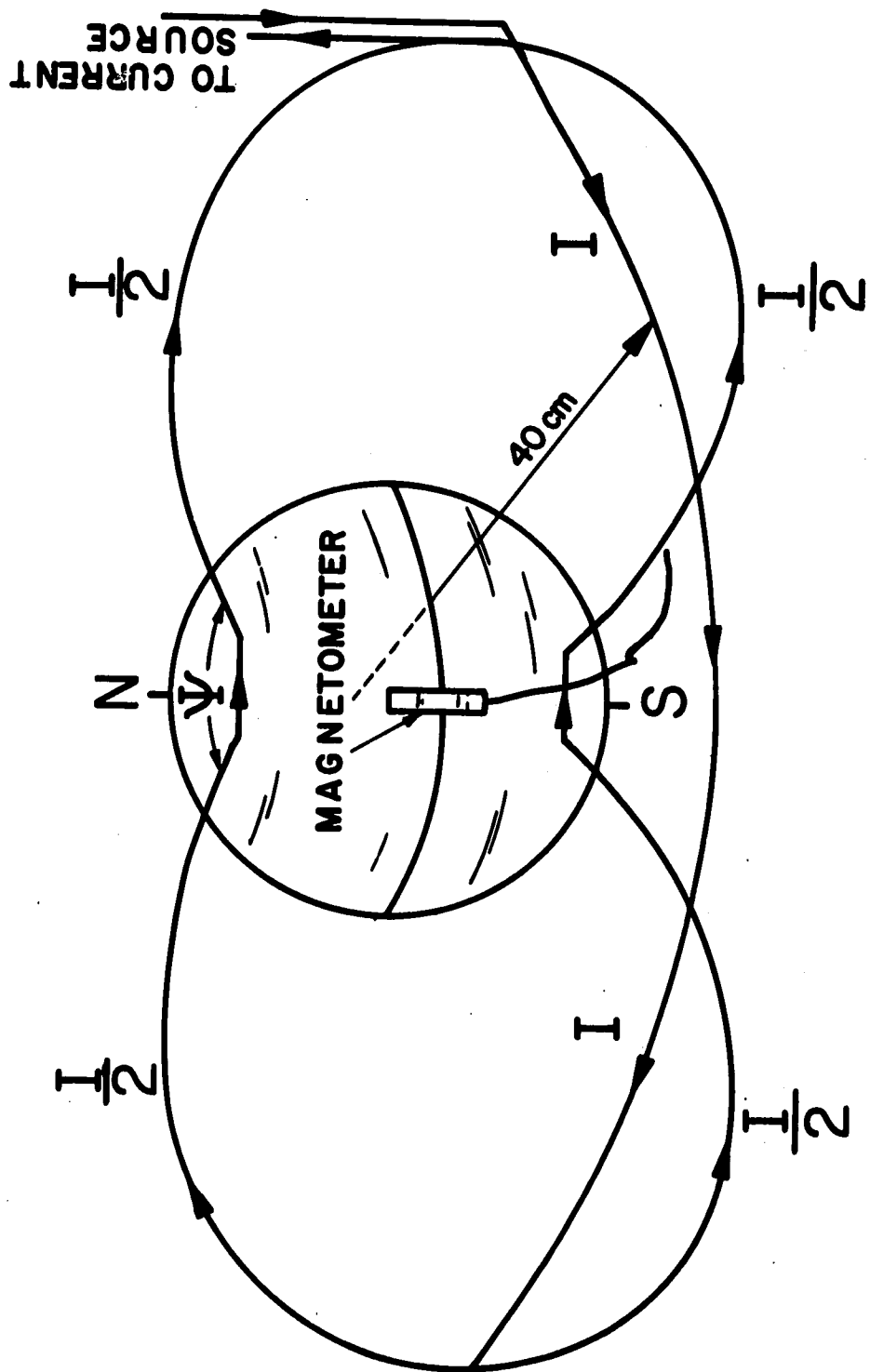
P54378

FIGURE 14

FIGURE 15

E. COMPARISON WITH MEASURED RECOVERY PHASES

In this section recovery phases calculated by the asymmetric ring current model are compared with measured recovery phases as observed at low-latitude magnetic observatories that are well spaced in longitude. The geographic longitude and geomagnetic latitude of the stations used in this study are listed in Table 2.

Ten sudden commencement storms from the five-year period 1957-1961 were chosen for this study. An attempt was made to select storms that had a quiet recovery phase, since the model used only provides for the decay of an asymmetric ring current presumably established at the height of the main phase (i.e., the model is not valid for storms in which the ring current belt is reformed during the recovery phase).

Since it was expected from the statistical study (Figure 12) that the asymmetry in the ring current belt would be centered about 1800 hours L.T., several storms were chosen that had $\sim$ 1800 L.T. for the hour of main phase decrease as observed at San Juan. If the asymmetry of the ring current is centered about 1800 hours, then the Honolulu and Guam magnetic observatories would be outside of the partial ring current system at the height of the main phase for these storms but would subsequently rotate under the asymmetry (provided the bulk of the energy of the ring current particles was in low energy protons). The differences in the recovery phases at San Juan, Honolulu and Guam should be most striking for this particular set of circumstances.

Calculated and measured recovery phases for the storm that began on July 15, 1959 are compared in Figure 16. The parameters that determine the asymmetric ring current for this storm are listed in Table 3, along with the parameters for the other storms analyzed. The initial position and size of the asymmetry, the values of S and A , and the initial position of the magnetic stations for the storm of July 15 are also given schematically in the top left corner of Figure 16.

For each station in Figure 16 the bars represent the hourly averaged values of H , where the zero levels for each hour are the 5-quiet-day values. The solid curve is the theoretical fit to the data. The curves used to determine the parameters for the asymmetric ring current are marked F (fitted) and the other curves are marked T (tested). The abscissa for each curve is the local time of the magnetic station.

There are two important things to notice about the curves of Figure 16. First, note the differences in the form of the recovery phases for the various stations. For example, the initial recovery rate at San Juan is more rapid than the initial recovery rate at Honolulu and Guam. As mentioned above, the recovery at Honolulu and Guam is retarded because these stations are initially outside the partial ring current system and subsequently rotate beneath the asymmetry.

The second thing to note about Figure 16 is the difference in the main phase decreases between stations

initially beneath the partial ring current system and
stations initially outside the system. For example, the
difference between the main phase decreases (normalized
to the equatorial plane) at San Juan and Tashkent is about
100 γ . This difference is fairly well reproduced by the
asymmetric ring current model.

Measured and computed recovery phases for the storm
that began on April 30, 1960 are compared in Figure 17.
Particularly striking in this case is the difference in
the form of the recovery phases as recorded at Honolulu
and Hermanus. These two stations are about 180° apart in
longitude, and for this storm Hermanus was directly be-
neath the partial ring current at the beginning of the
recovery phase.

Measured and computed recovery phases for the other
storms analyzed are compared in Figures 18 through 25.
Similar comments about the differences in the recovery
phases and magnitudes of main phase decreases can be made
for some of these curves. However, as these figures show,
this simple asymmetric ring current model is only partially
successful in fitting some storms.

The uncertainty in the zero level for ΔH could be
one reason for the apparent failure of the asymmetric ring
current model to fit the recovery phases of weak storms.
As mentioned in the previous section, the zero levels for
the measured ΔH are the 5-quiet-day values. By subtract-
ing out the 5-quiet-day averages, we are attempting to
eliminate the quiet day diurnal variation from the storm

field. There is, of course, some uncertainty in this
process, since the quiet day variation changes slightly
from day to day. Also, one is not sure that the iono-
spheric current patterns causing the quiet day variation
remain the same during a magnetic storm.

To get an idea of the uncertainties involved in
defining the zero level for the storm field, we have
plotted in Figures 26 through 28 the storm of July 15, as
observed at San Juan, Tucson and Honolulu, using three
different definitions of zero. In the first set of data,
the hourly average of the five quiet days in July is de-
fined as zero. For the second set of data, we have used
the hourly averages of the day preceding the storm. For
the third set, we have not tried to subtract out the
quiet day diurnal variation. The average over all hours
for the ten quiet days in July is defined as zero.

These figures show that during the daylight hours
the uncertainty in the zero level is greater than during
the night hours.

A source of error that affects all the comparisons
between measured and computed recovery phases is the
neglect of the diamagnetic effect of the ring current
particles that make up the asymmetry in the ring current
belt. For the symmetric ring current, the magnetization
of the ring current particles cancels about a third of
the main phase decrease caused by the drift currents
(Dessler and Parker, 1959). By assuming the same correc-
tion is necessary for the particles in the asymmetry, one

can derive partial ring current functions that take account
of the diamagnetic effect. In Figure 29 a "corrected"
partial ring current function ($\Psi = 140°$) is compared with
the corresponding function used in this study. As can
be seen from this figure, the two partial ring current
functions differ only at local times opposite to φ_0. For
these local times the magnetic field of the partial ring
current is much less than the magnetic field of the symmetric
current, so the form of the recovery phase would not be
greatly changed by inclusion of the diamagnetic effect in
the asymmetric ring current model.

In computing the partial ring current functions by
the scale model of the current system, the contribution to
ΔH from the "ionospheric" element was found to be much less
important than the contribution from the current flowing
along the field lines. Changes in the position of the
copper braid of the scale model produced little or no effect
on the magnetometer, but movements of the dipole arms of
the current system were easily detected.

Because of the diamagnetic earth, the ionospheric
element of the partial ring current system probably contri-
butes very little to the main phase decrease observed at
an equatorial station. Even discounting the diamagnetism
of the earth, the contribution of the ionospheric element
is only a fraction of the contribution of the equatorial
element. The earth current below the ionospheric element
further reduces this contribution, since the induced current
is antiparallel with the ionospheric current. The

ionospheric current flows at an altitude of $\approx$ 100 km, and
the earth current flows at a depth of less than $\approx$ 260 km
(Chapman, 1951), so that the separation between the two
oppositely directed currents is less than $\approx$ 360 km. The
magnetic effect is negligible at an equatorial station
several thousand kilometers from the two currents.

The magnetic effect of earth currents induced in the
vicinity of the low latitude magnetic observatories are
lumped into the amplitudes S and A .

TABLE 2. The geographic longitude and geomagnetic latitude
of the magnetic observatories used in this thesis.

MAGNETIC OBSERVATORY	GEOGRAPHIC LONGITUDE	GEOMAGNETIC LATITUDE
M'BOUR	17.0° W	21.3° N
SAN JUAN	66.1° W	29.9° N
TUCSON	110.8° W	40.4° N
HONOLULU	158.0° W	21.1° N
GUAM	144.9° E	4.0° N
TASHKENT	69.3° E	32.0° N
ADISS-ABABA	38.8° E	5.4° N
HERMANUS	19.2° E	33.3° S

FIGURE 16:   Comparisons between measured and computed

recovery phases for the storm that began

on July 15, 1959. The solid bars repre-

sent the measured hourly averages, and

the curves are the computed recovery

phases. The zero level for each hour is

defined by the monthly 5-quiet-day average

values. The diagram in the top left corner

shows the positions of the magnetic sta-

tions at the beginning of the recovery

phase. The values of S and A , and the

size and initial position of the asymmetry

in the ring current belt are also represented

schematically by this diagram.

FIGURES 17-25:   Comparisons between measured and computed

recovery phases for the storms that began on:

                  17)   April 30, 1960,
                  18)   January 21, 1957,
                  19)   September 29, 1957,
                  20)   February 11, 1958,
                  21)   July 27, 1961,
                  22)   October 28, 1961,
                  23)   December 3, 1958,
                  24)   November 6, 1957,
           and   25)   September 13, 1957.
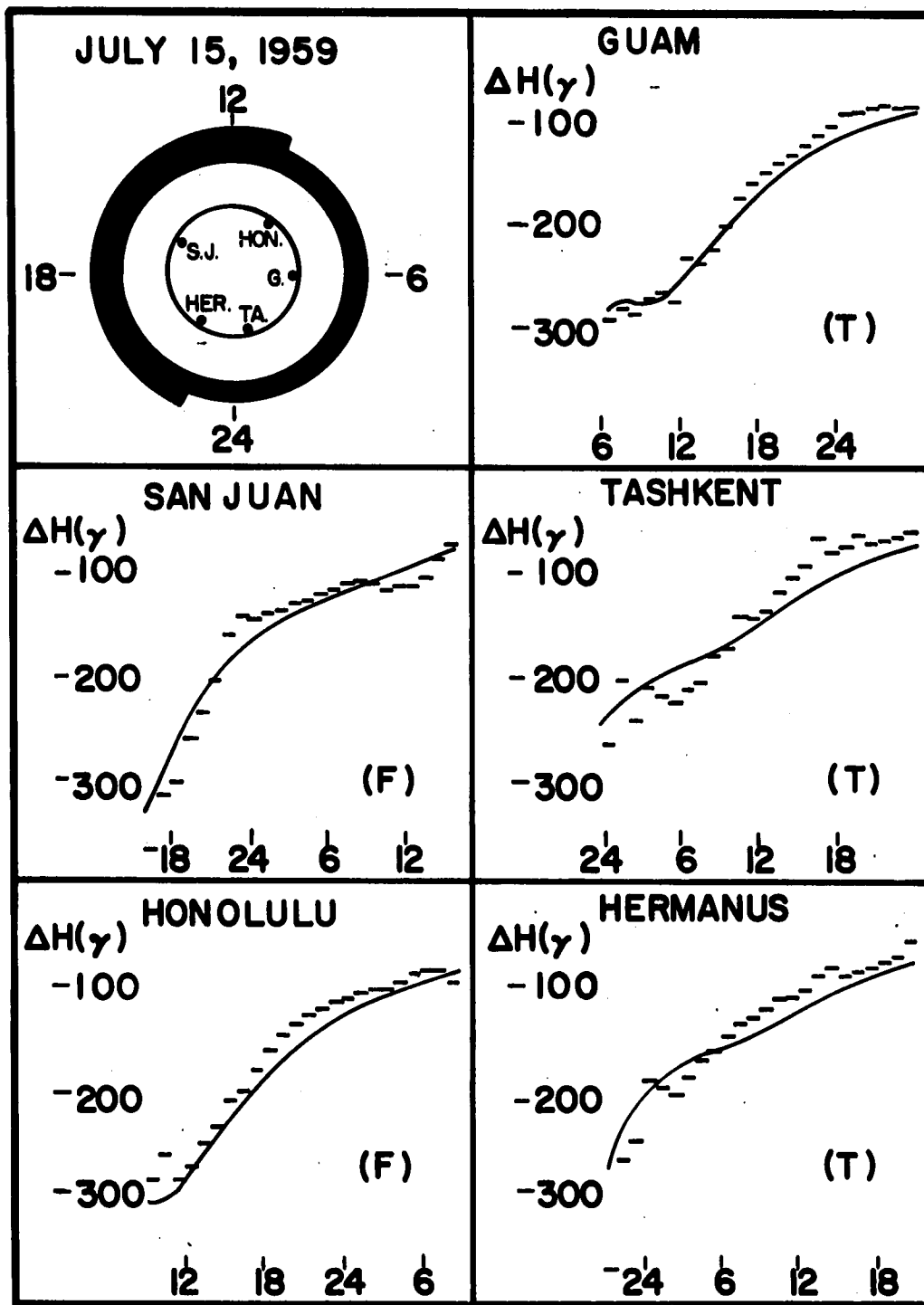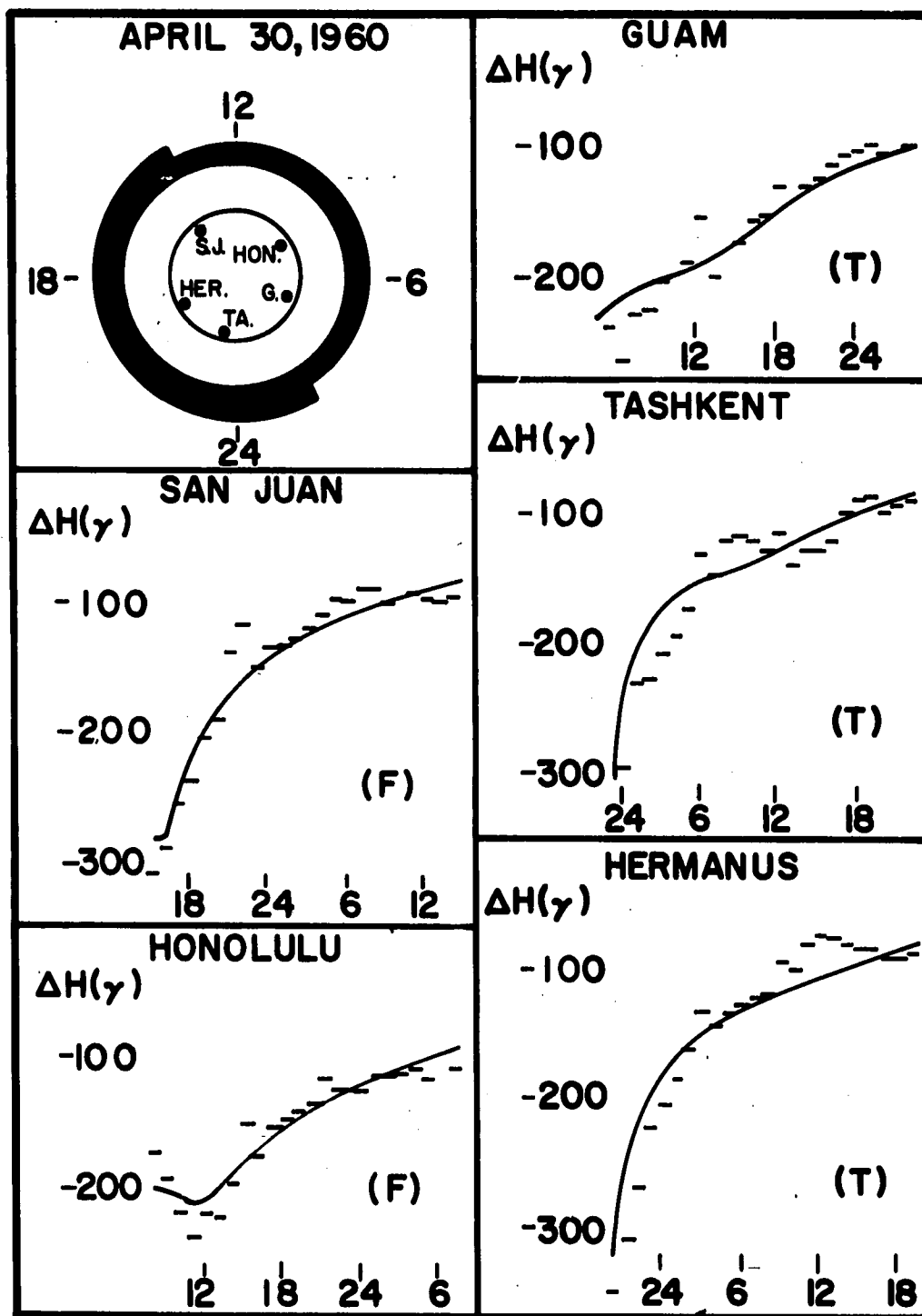
FIGURE 16

FIGURE 17

JANUARY 21, 1957

TUCSON
ΔH(γ)
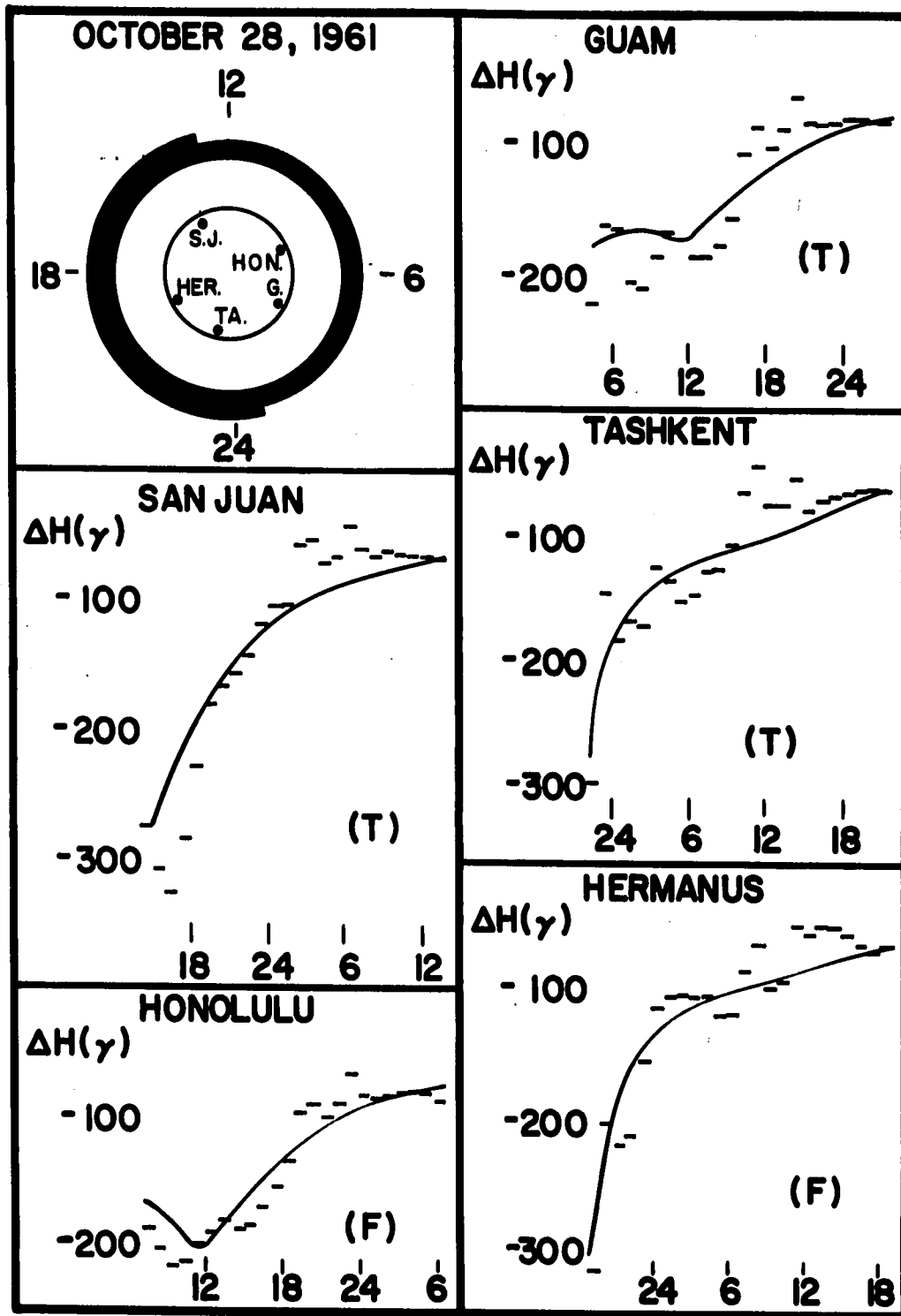
SAN JUAN
ΔH(γ)

HONOLULU
ΔH(γ)
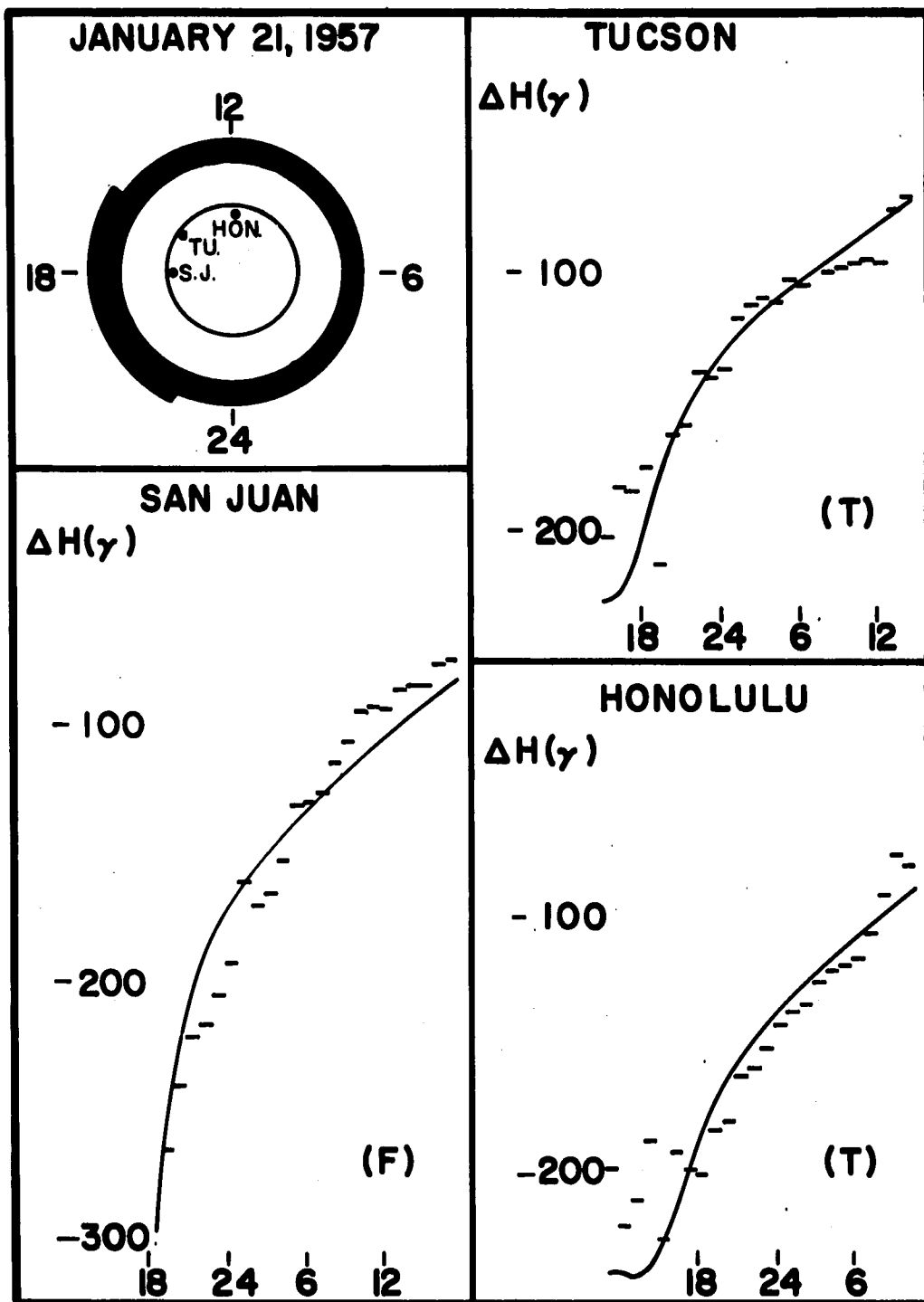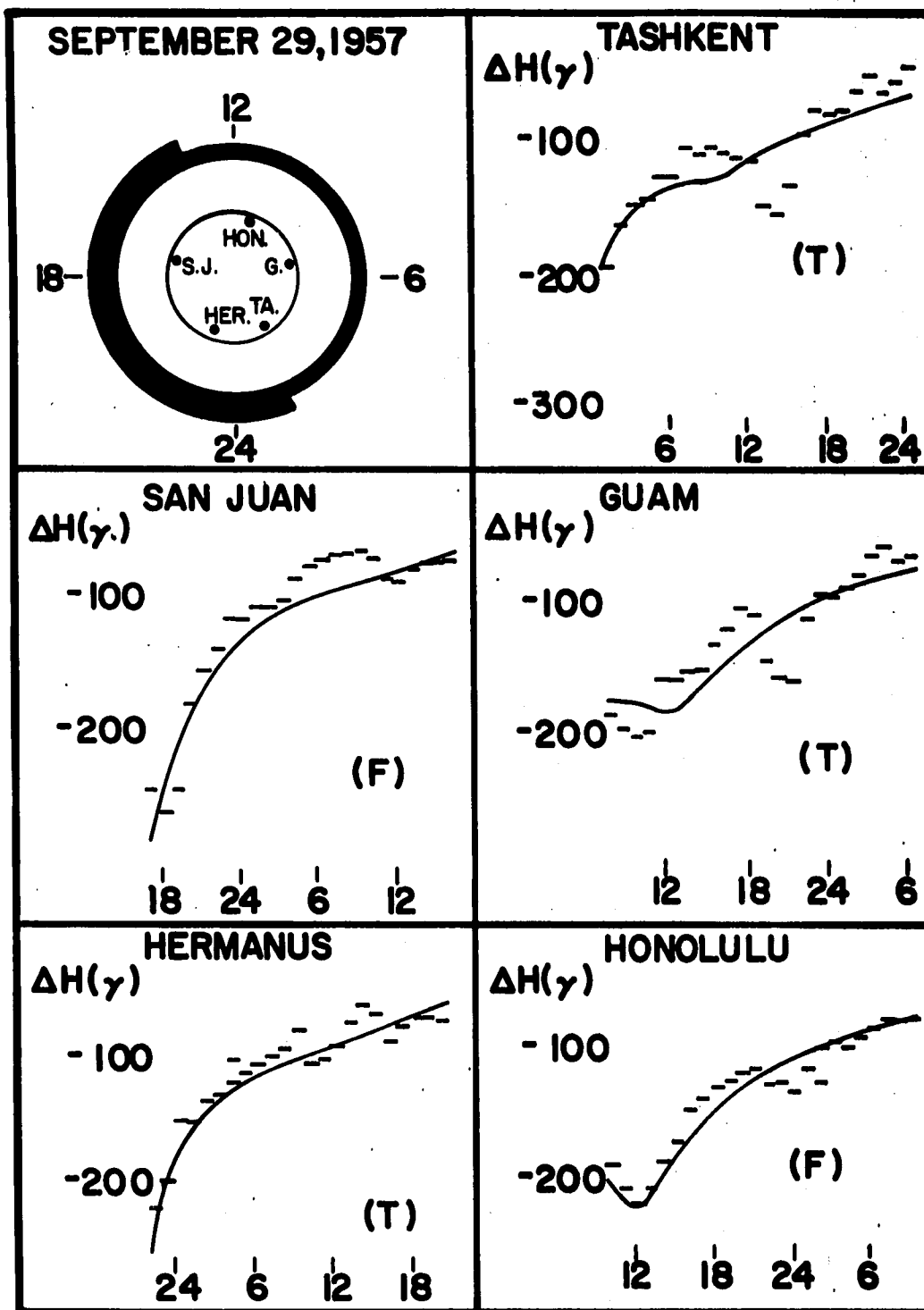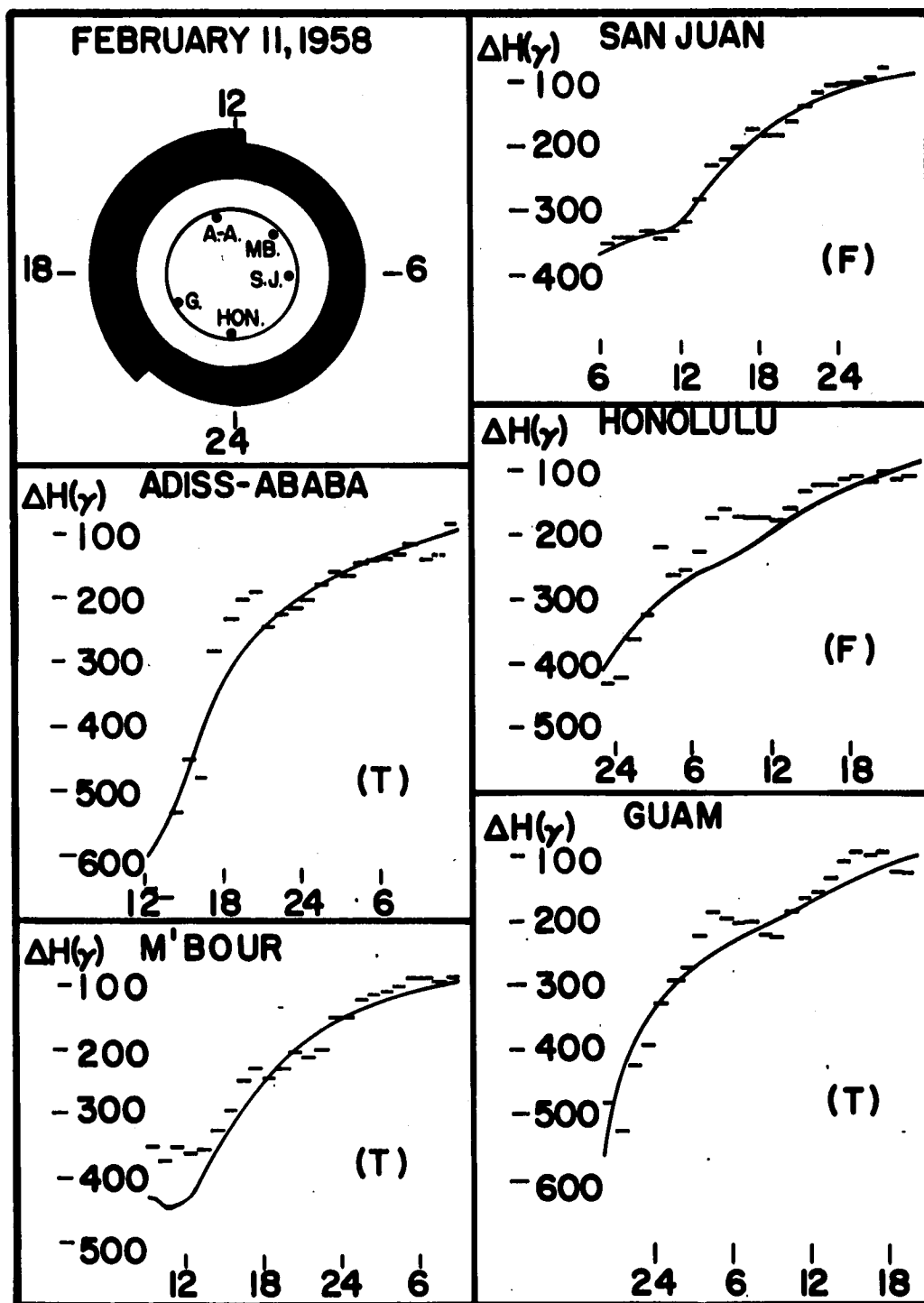
P 54402

FIGURE 18
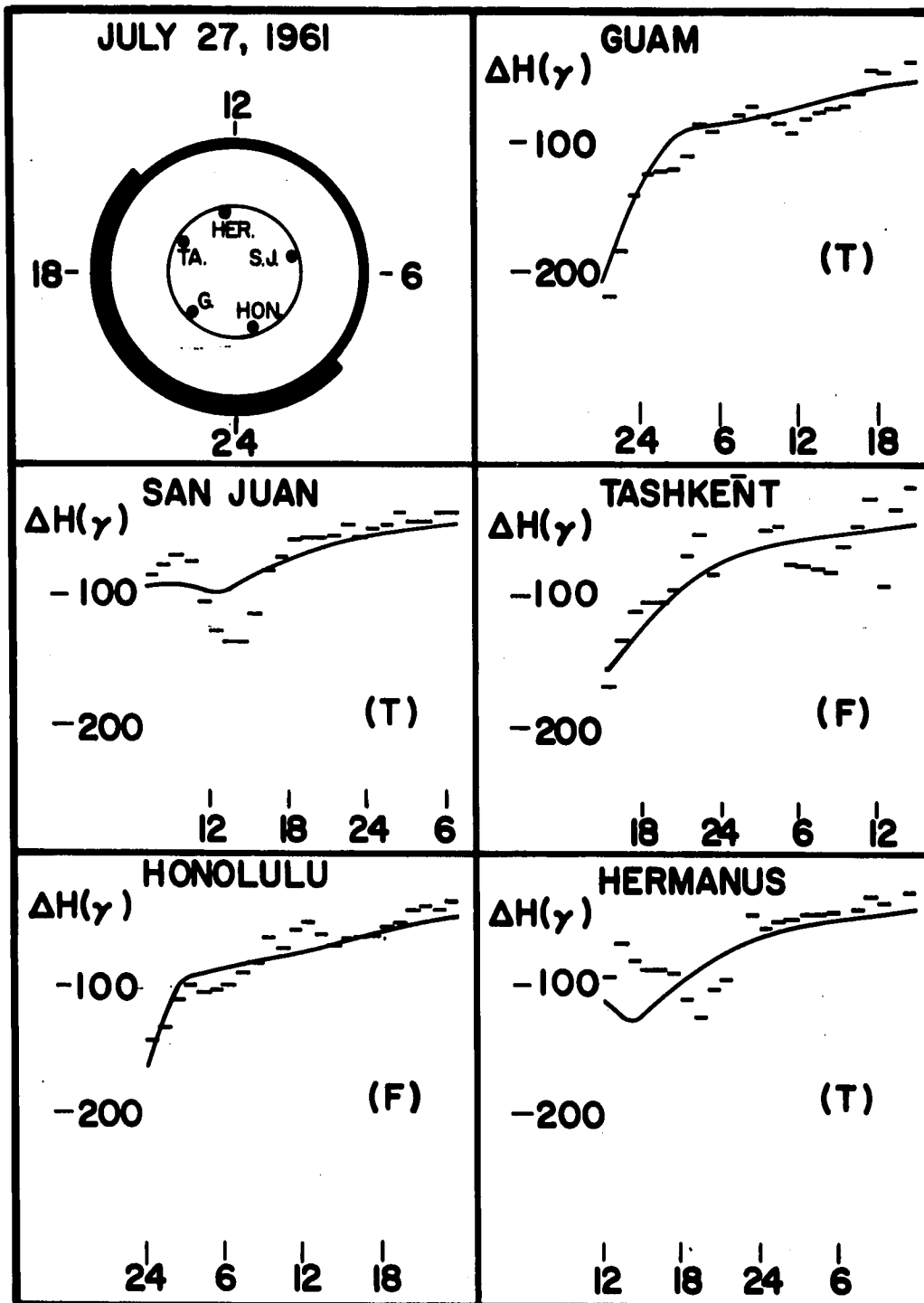
FIGURE 19

FIGURE 20

FIGURE 21

FIGURE 22

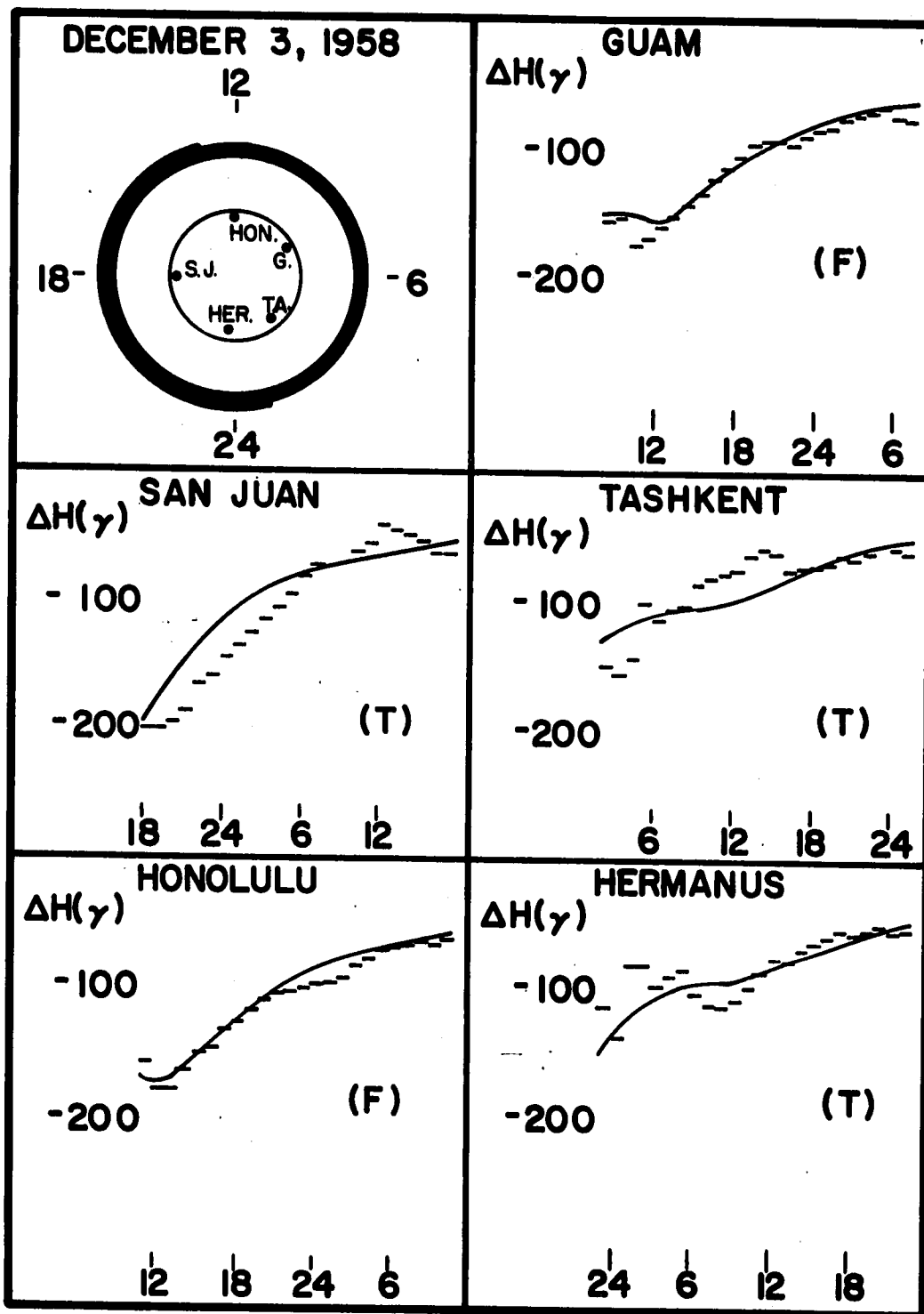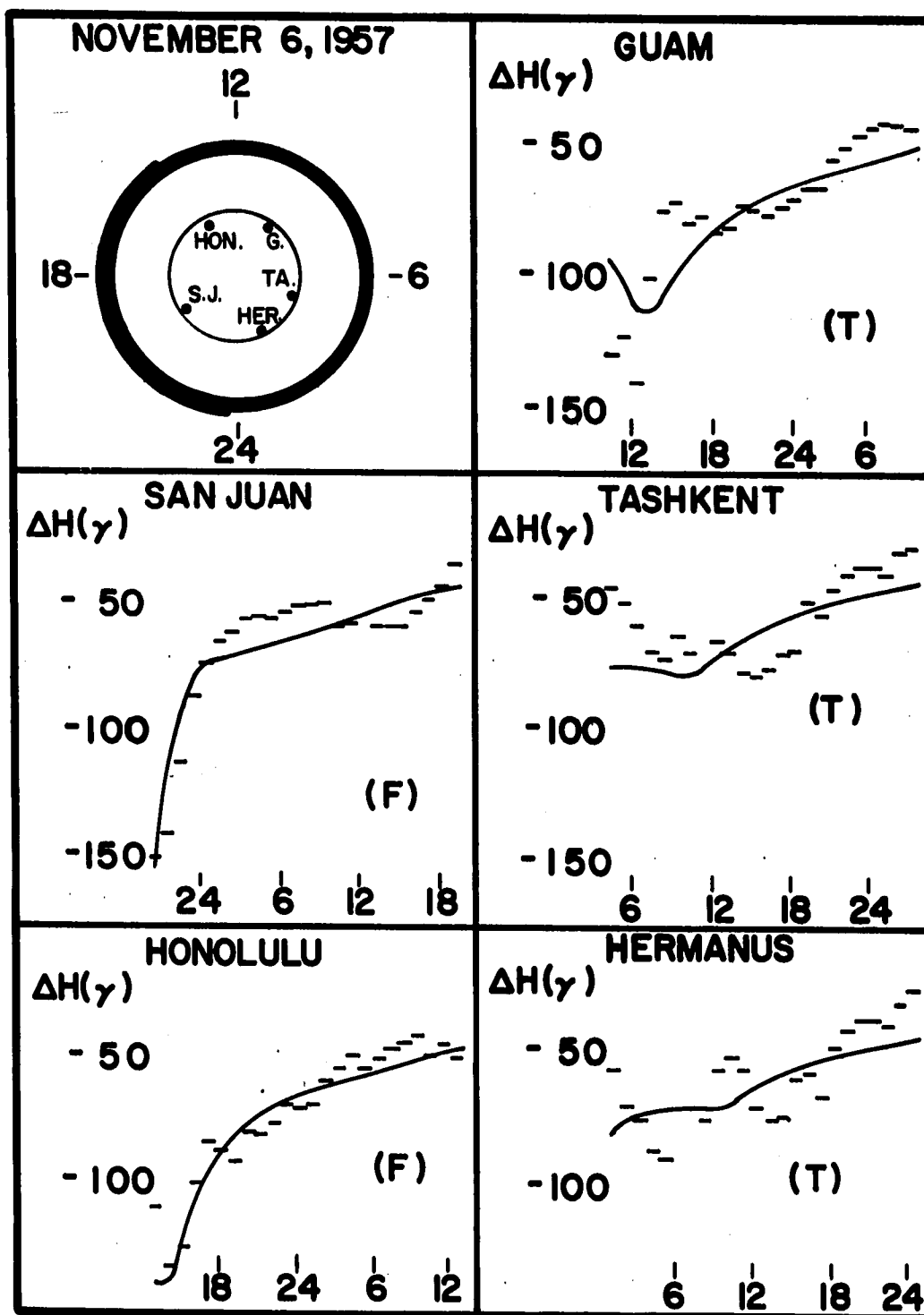FIGURE 23

P54414

FIGURE 24

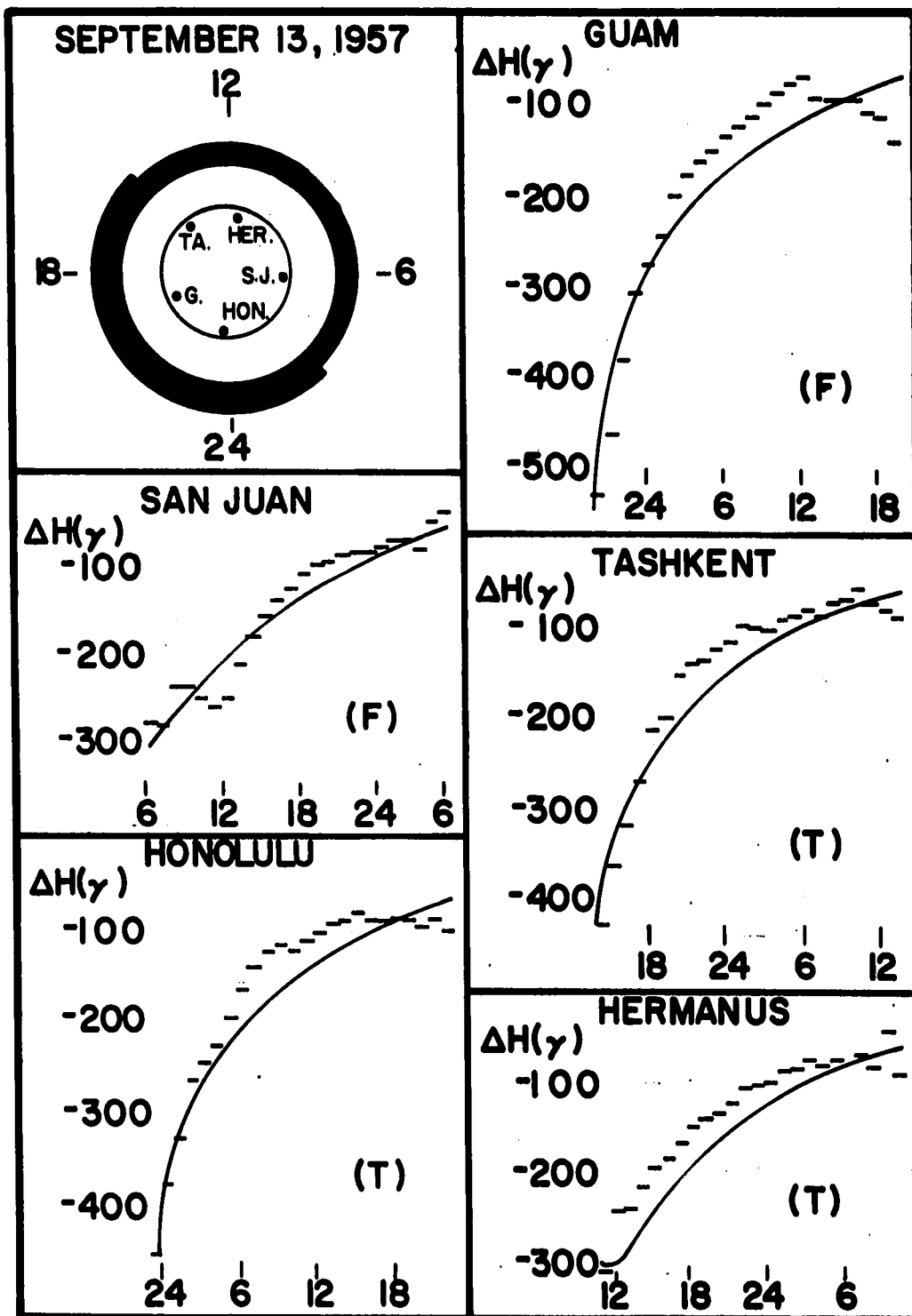FIGURE 25
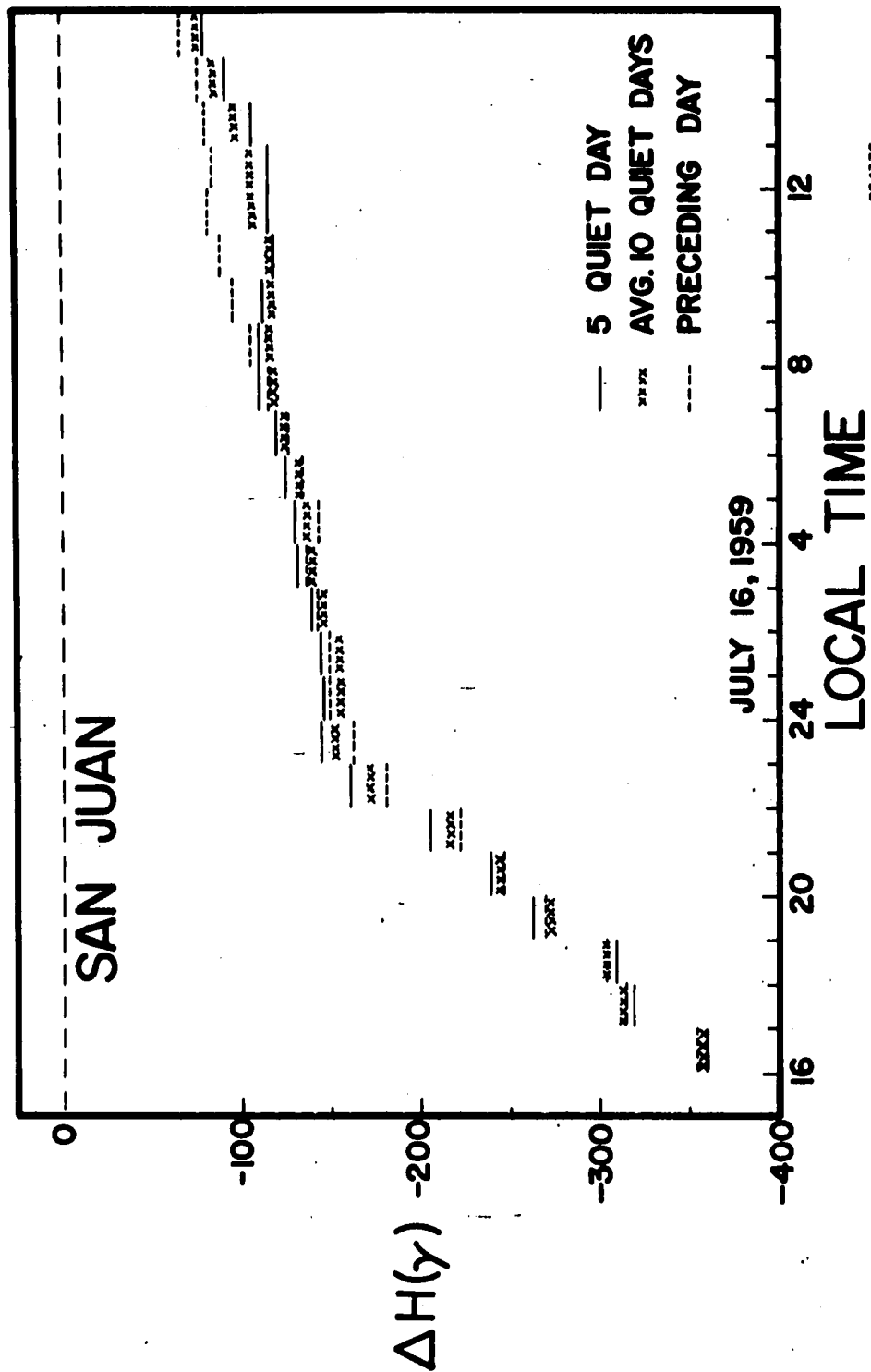
P54415

TABLE 3. The asymmetric ring current parameters for the storms analyzed in this thesis.

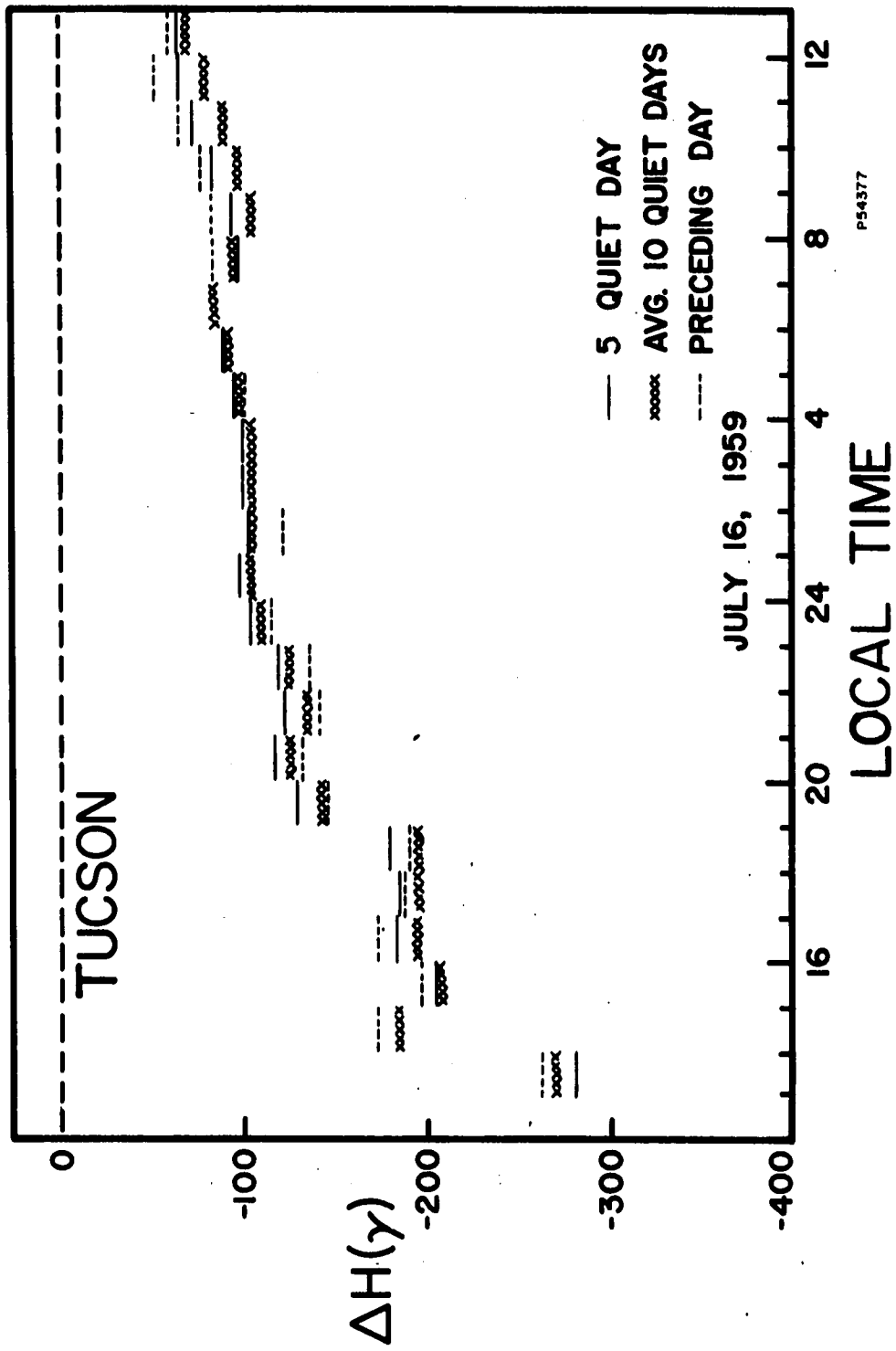| STORM DATE	A	S	τ_P(hrs.)	τ_S(hrs.)	$v\left(\dfrac{\text{hrs.L.T.}}{\text{hrs.U.T.}}\right)$	Y(degs.)	φ_o(degs.)
JULY 15, 1959	100	300	6	20	0.3	180	1630
APRIL 30, 1960	180	240	3	27	0.5	180	2000
JAN. 21, 1957	100	260	4	24	0.3	100	1900
SEPT. 29, 1957	150	200	4	24	0.4	180	1930
FEB. 11, 1958	200	460	6	15	0.3	140	1830
JULY 27, 1961	100	120	4	27	0.3	100	2100
OCT. 28, 1961	180	200	5	24	0.3	180	1900
DEC. 3, 1958	70	160	6	24	0.3	180	1900
NOV. 6, 1957	100	100	3	35	0.6	140	1900
SEPT. 13, 1957	160	370	2	15	0.6	180	2100

FIGURES 26-28:   The storm of July 15, 1959, using three
                  different zero definitions. The solid
                  bars correspond to defining the July
                  5-quiet-day hourly averages as zero. The
                  dashed bars correspond to defining the
                  hourly averages of the preceding day as
                  zero. For the x bars, the average over
                  all hours for the ten quiet days in July
                  is defined as zero.

FIGURE 29:   The partial ring current function ($\Psi = 140°$)
                  that has been corrected for the diamagnetic
                  effect of the ring current particles. The
                  corrected function differs from the
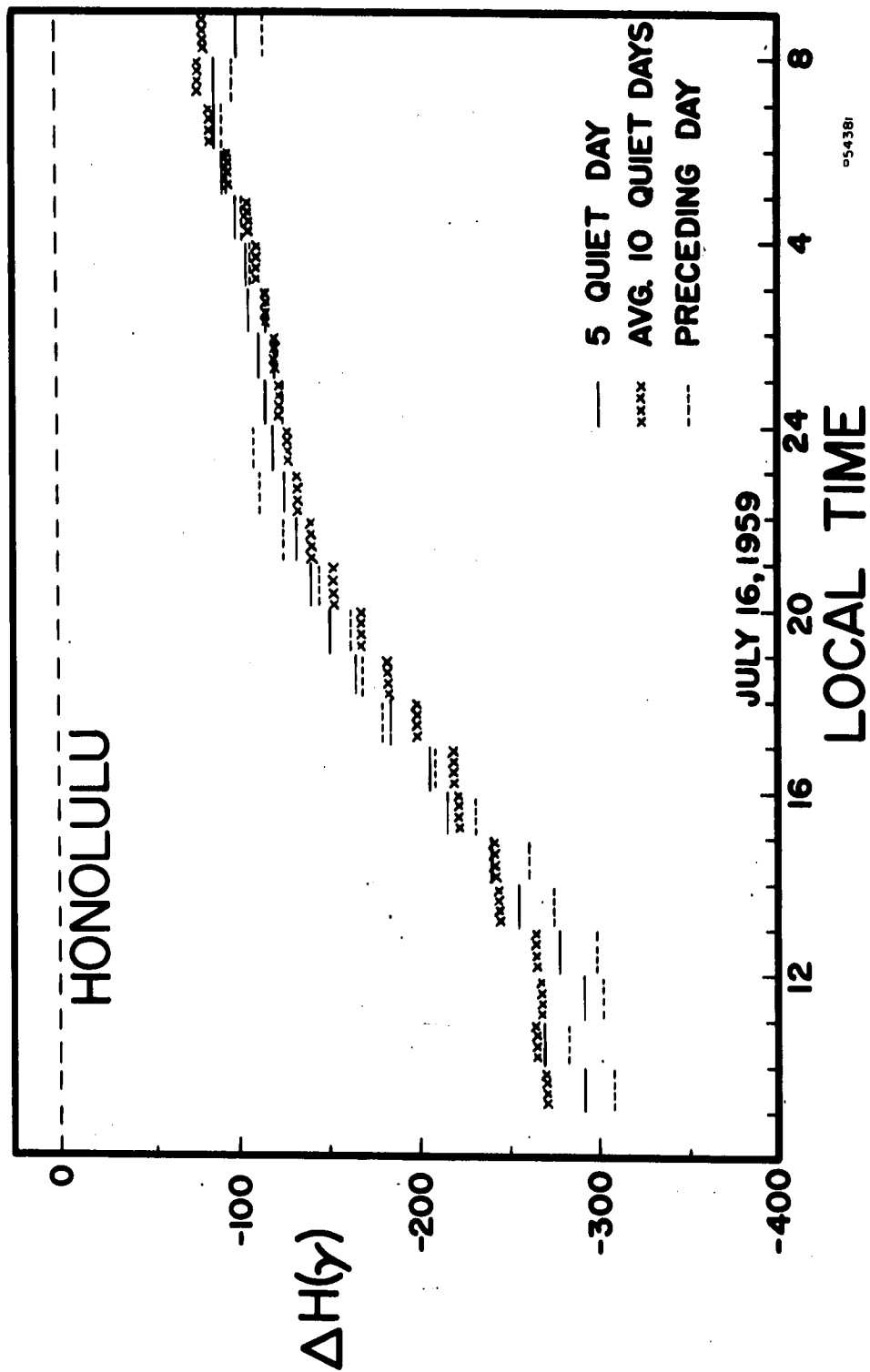   uncorrected function at local times opposite
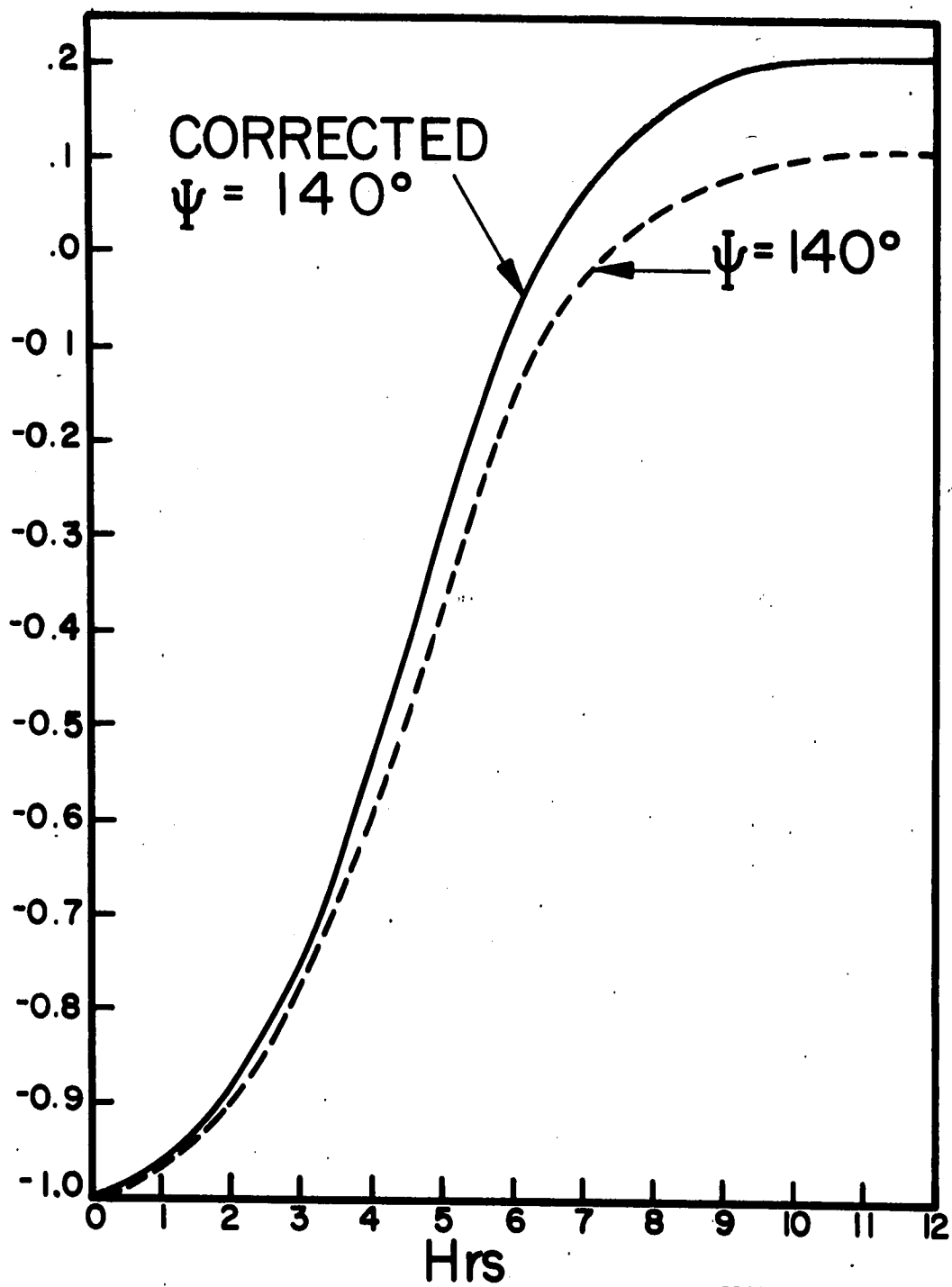   to φ_o .

FIGURE 26

FIGURE 27

FIGURE 28

FIGURE 29